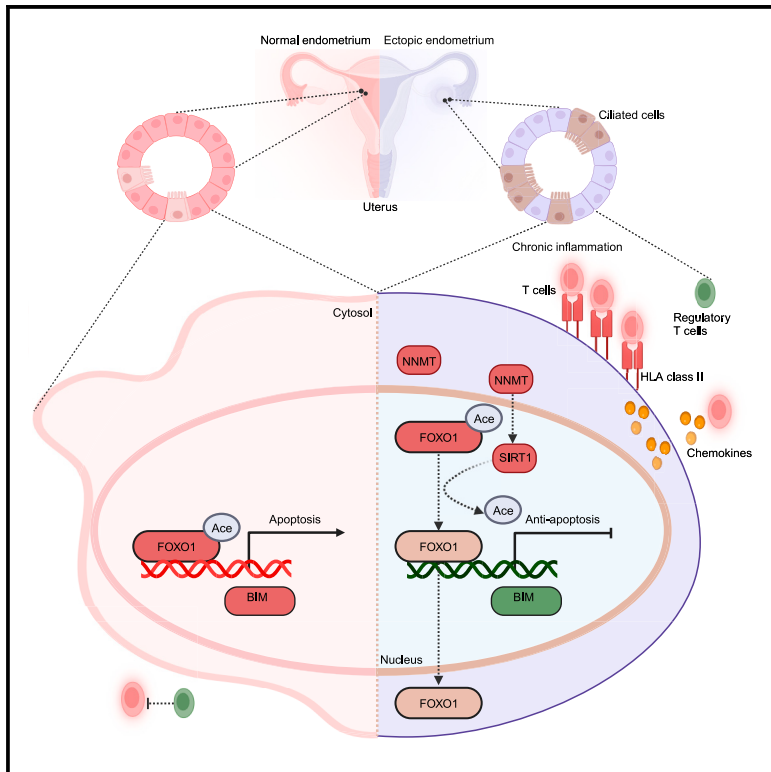


Single-cell analysis reveals insights into epithelial abnormalities in ovarian endometriosis

Graphical abstract



Authors

Jia Yan, Ling Zhou, Mengya Liu, ..., Lin Dai, Xiaohong Chang, Fuchou Tang

Correspondence

changxiaohong@pkuph.edu.cn (X.C.), tangfuchou@pku.edu.cn (F.T.)

In brief

Yan et al. generated a single-cell endometriosis atlas and revealed that ciliated cells in eutopic and ectopic endometrium suppress apoptosis through reduced estrogen sulfotransferase expression. In ectopic lesions, epithelial cells further adapted to survive by resisting apoptosis via NNMT and driving chronic inflammation through the HLA class II complex.

Highlights

- Eutopic and ectopic endometrium upregulate the percentage of ciliated cells
- The ciliated cells in patients exhibit decreased SULT1E1 expression
- Epithelial cells in endometriotic lesions resist apoptosis through NNMT-FOXO1-BIM pathway
- Epithelial cells in endometriotic lesions stimulate CD4⁺ T cells via HLA class II complex



Article

Single-cell analysis reveals insights into epithelial abnormalities in ovarian endometriosis

Jia Yan,^{1,2,3,6} Ling Zhou,^{4,6} Mengya Liu,^{1,3,6} Honglan Zhu,^{4,6} Xin Zhang,^{1,6} E. Cai,^{4,6} Xueqiang Xu,^{1,2,3} Tinghan Chen,¹ Hongyan Cheng,⁴ Jun'e Liu,^{1,3} Shang Wang,⁴ Lin Dai,⁵ Xiaohong Chang,^{4,*} and Fuchou Tang^{1,2,3,7,*}

¹School of Life Sciences, Biomedical Pioneering Innovation Center, Peking University, Beijing 100000, China

²Academy for Advanced Interdisciplinary Studies, Peking University, Beijing 100000, China

³Ministry of Education Key Laboratory of Cell Proliferation and Differentiation, Peking University, Beijing 100000, China

⁴Department of Obstetrics and Gynecology, People's Hospital, Peking University, Beijing 100044, China

⁵Department of Pathology, People's Hospital, Peking University, Beijing 100044, China

⁶These authors contributed equally

⁷Lead contact

*Correspondence: changxiahong@pkuph.edu.cn (X.C.), tangfuchou@pku.edu.cn (F.T.)

<https://doi.org/10.1016/j.celrep.2024.113716>

SUMMARY

Ovarian endometriosis is characterized by the growth of endometrial tissue within the ovary, causing infertility and chronic pain. However, its pathophysiology remains unclear. Utilizing high-precision single-cell RNA sequencing, we profile the normal, eutopic, and ectopic endometrium from 34 individuals across proliferative and secretory phases. We observe an increased proportion of ciliated cells in both eutopic and ectopic endometrium, characterized by a diminished expression of estrogen sulfotransferase, which likely confers apoptosis resistance. After translocating to ectopic lesions, endometrial epithelium upregulates nicotinamide N-methyltransferase expression that inhibits apoptosis by promoting deacetylation and subsequent nuclear exclusion of transcription factor forkhead box protein O1, thereby leading to the downregulation of the apoptotic gene BIM. Moreover, epithelial cells in ectopic lesions elevate HLA class II complex expression, which stimulates CD4⁺ T cells and consequently contributes to chronic inflammation. Altogether, our study provides a comprehensive atlas of ovarian endometriosis and highlights potential therapeutic targets for modulating apoptosis and inflammation.

INTRODUCTION

The endometrium, the mucous layer lining the uterus, undergoes dynamic changes during the menstrual cycle driven by estrogen and progesterone signaling.¹ Histomorphology categorizes the menstrual cycle into a menstrual phase, a proliferative phase, and a secretory phase (Figure 1A).² Endometriosis is characterized by the presence and growth of endometrial-like tissue outside the uterine cavity and is classified into three types based on its location: ovarian endometriosis, peritoneal endometriosis, and deep infiltrating endometriosis.³ Approximately 10% of women of reproductive age are affected by endometriosis, with symptoms such as chronic pelvic pain, dysmenorrhea, painful intercourse, and infertility.⁴ Current clinical treatments for endometriosis include hormonal drugs, such as oral contraceptives and progestogens, and surgical removal. However, the medical therapies have limited efficacy and unwanted side effects, including headache, weight gain, and irregular bleeding. Furthermore, both interventions are associated with high rates of recurrence.⁵ Therefore, unraveling deeper pathophysiological mechanisms of endometriosis is critical for developing more effective treatments.

While previous bulk and single-cell genomic studies have yielded insights into endometriosis, some methodological issues remain unsolved.^{6–8} Small sample sizes have hindered statistical analysis stratified by endometriosis subtypes.⁶ In this study, due to the high prevalence and significant ovarian damage, we focus exclusively on samples of ovarian endometriosis. Additionally, obtaining representative normal and eutopic tissues from healthy controls and patients within the same menstrual phase has been challenging. This difficulty has led to an underestimation of initial triggers of endometriosis.⁸ Lastly, few studies have rigorously addressed biases related to phase and individual variability in their comparisons of ectopic and eutopic tissues. These limitations have hindered a comprehensive understanding of the pathophysiology of endometriosis.

In this study, we applied a high-precision single-cell RNA sequencing method, single-cell tagged reverse transcription sequencing (STRT-seq), to profile normal endometrium from 11 healthy women and eutopic endometrium and ectopic endometrium from 23 women with ovarian endometriosis. Our study delved into the important roles of epithelial cells in the pathogenesis of endometriosis by rigorously controlling for phase and



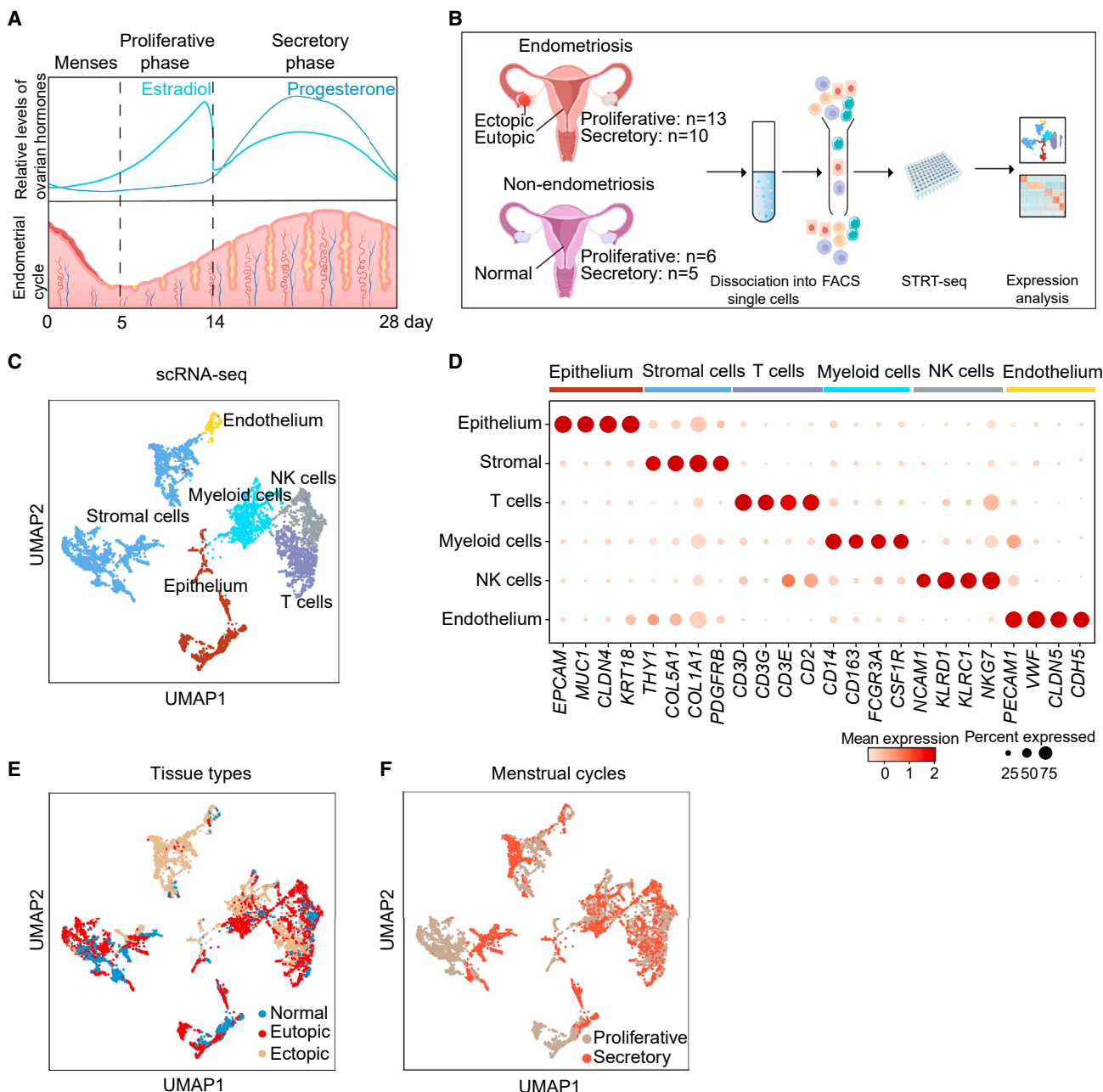
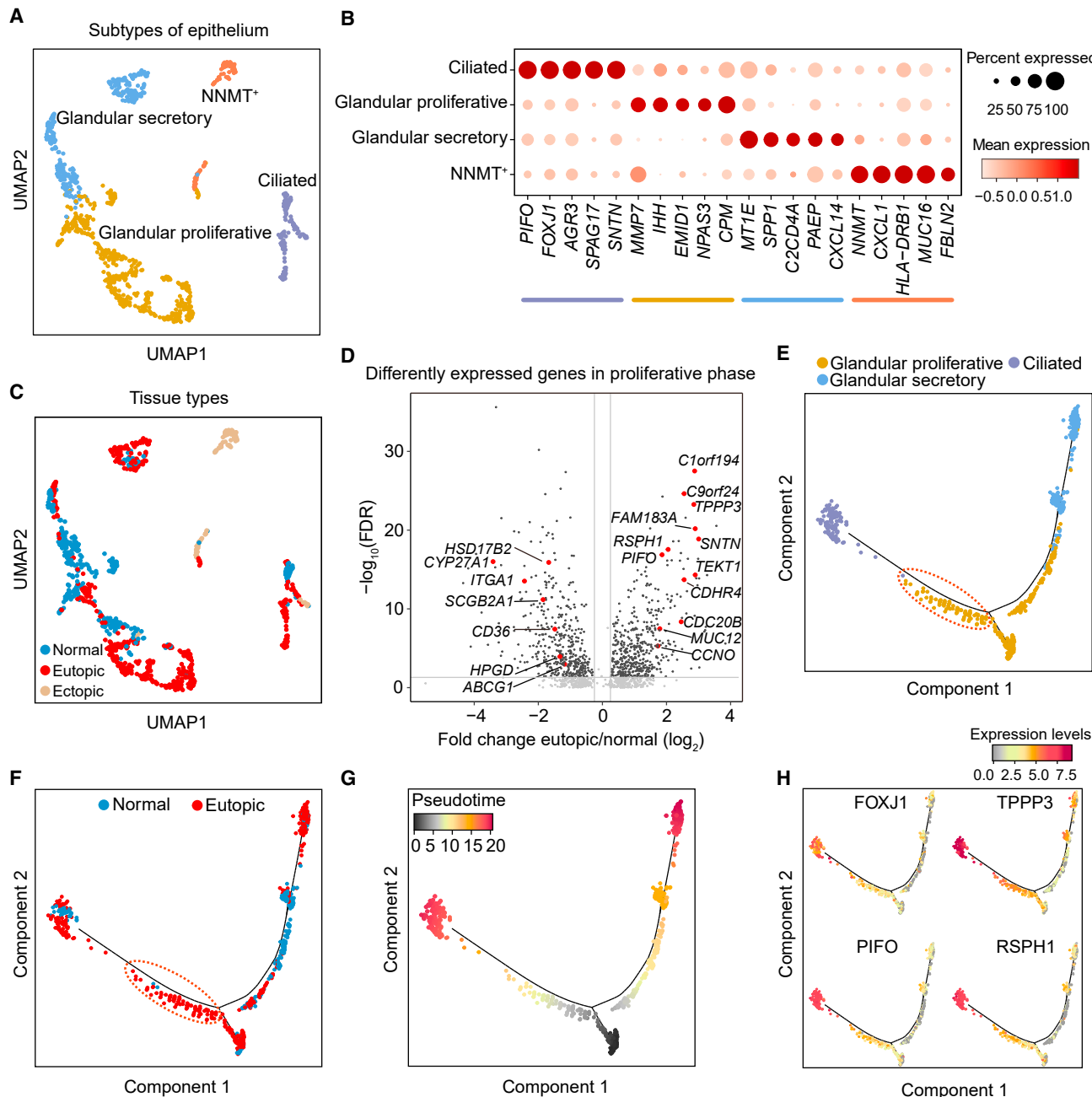


Figure 1. Single-cell profiling of endometriosis samples and healthy controls in different menstrual phases

- (A) Schematic illustration of the human endometrium showing the morphological changes and hormonal changes throughout the menstrual cycle.
 - (B) Schematic of design and processing of samples. Normal samples were obtained from endometrium of individuals without endometriosis. Eutopic and ectopic samples were obtained from individuals with endometriosis. Proliferative, proliferative phase; secretory, secretory phase. n means number of individuals.
 - (C) Uniform manifold approximation and projection (UMAP) for a total of 7,030 single cells from normal and endometriosis tissues.
 - (D) Dot plot showing Z score-scaled mean expression of marker genes expressed in main cell types.
 - (E) UMAP representations colored by sampling sites.
 - (F) UMAP representations colored by menstrual cycle annotated by tissue histomorphology.
- See also [Figure S1](#).

individual variations. Our study highlighted the dysregulation of ciliated cells in patients. We uncovered the role of nicotinamide N-methyltransferase (NNMT) in inhibiting apoptosis and the

immunoregulatory function of epithelial cells in ectopic lesions. These findings advance our understanding of the causal and pathological features of endometriosis.

**Figure 2. Epithelial heterogeneity in normal and endometriosis samples**

- (A) UMAP of subclustered epithelial cells from all individuals. Each color represents a subtype of cells.
- (B) Dot plot showing the Z score-scaled mean expression of marker genes of each epithelial subset. The line under the genes represents the cell types corresponding to (A).
- (C) UMAP representations colored by sampling sites.
- (D) Volcano plot comparing eutopic to normal epithelial cells from 7 patients and 4 normal individuals at proliferative phase. Significantly discriminatory genes ($\text{false discovery rate } [\text{FDR}] < 0.05$, $\log_2[\text{fold change}] > 0.25$) are colored in black.
- (E) Pseudotemporal trajectory representing the tissue types of epithelial cells. Epithelial cells at proliferative phase differentiating into ciliated cells are circled.
- (F) Pseudotemporal trajectory representations colored by sampling sites. Epithelial cells at proliferative phase differentiating into ciliated cells are circled.
- (G) Pseudotemporal trajectory representations colored by pseudotime.
- (H) Pseudotemporal trajectory representations colored by expression level ($\ln(\text{TPM}+1)$) of ciliated genes.

See also Figure S2.

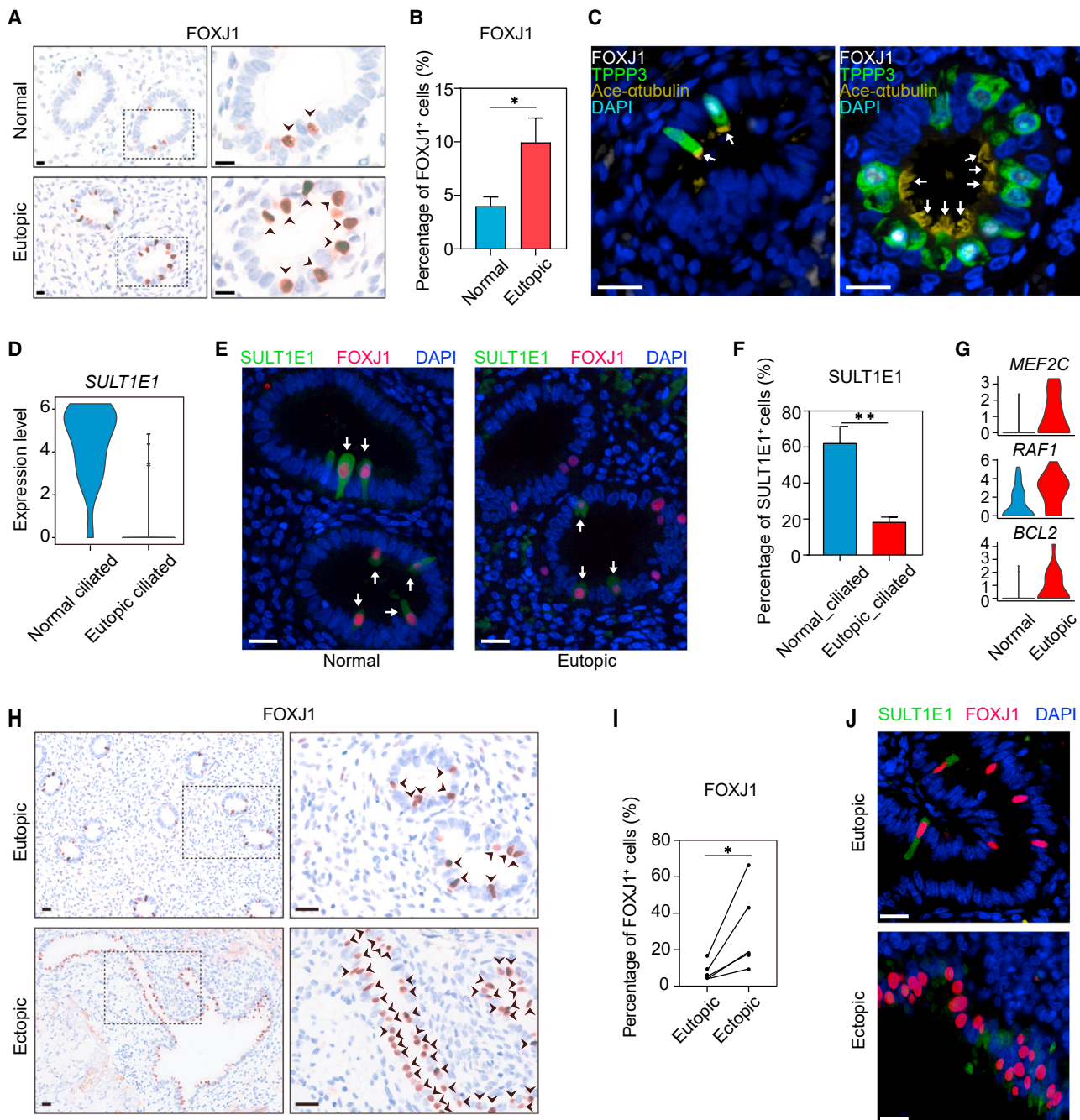


Figure 3. Characterization of ciliated cells in eutopic and ectopic endometriosis samples

- (A) Representative images of immunohistochemistry (IHC) staining for FOXJ1 (brown, arrow). Nuclei: blue. Close-up images (right) contain cells seen in the left black dashed box of the main image. Scale bar, 10 μ m.
- (B) Bar plot showing the percentage of FOXJ1⁺ cells in epithelial cells from 5 patients and 6 normal controls at proliferative phase. Data are represented as mean with SEM. Two-tailed t test was used to derive p values. *p < 0.05.
- (C) Immunofluorescence staining of eutopic and normal tissue sections. FOXJ1, TPPP3, and acetylated α -tubulin are markers of ciliated cells and colored by white, green, and yellow respectively. Nuclei: blue. Scale bar, 20 μ m. Cells with ciliated structure are labeled by white arrows.
- (D) Violin plot showing the downregulated expression of SULT1E1 in ciliated cells in eutopic endometrium relative to normal controls (FDR < 0.05, log₂[fold change] > 0.25).
- (E) Immunofluorescence staining showing the co-localization of SULT1E1 (green) with ciliated cells (FOXJ1⁺, red). Nuclei: blue. Scale bar, 20 μ m.
- (F) Bar plot showing the percentage of SULT1E1⁺ cells in ciliated cells (FOXJ1⁺) in sections from 3 patients and 3 normal controls. Data are represented as mean with SEM. Two-tailed t test was used to derive p values. **p < 0.01.

(legend continued on next page)

RESULTS

Single-cell transcriptome profiling of endometriosis

We collected endometrial samples from 23 patients diagnosed with ovarian endometriosis and 11 healthy individuals (Figure 1B; Table S1). Representative normal endometrial samples were obtained from individuals without endometriosis. To account for the dynamic changes in the endometrium, we collected samples from both the proliferative and secretory phases, enabling direct comparisons between eutopic and normal endometrium at the same phases. The menstrual phases of the samples were accurately determined using histomorphology, a highly precise diagnostic method.⁹ For comparison purposes, matched samples of eutopic endometrium and ectopic lesion were collected from the same patients to exclude individual differences. To capture the heterogeneity of the cellular landscape, epithelial cells, stromal cells, and immune cells were isolated and sorted into single cells by using the fluorescence-activated cell sorting method. These single cells were subsequently sequenced by a high-precision single-cell transcriptomics technology—STRT-seq, which allowed us to detect a higher number of genes and unique transcripts in individual cells.

After strict quality control and filtration, we obtained a total of 7,030 cells with a median of 101,675 unique transcripts and 4,620 genes per cell (Figure S1A; Table S1). Cells were assigned to 6 cell types based on the expression of well-known markers and enriched biological processes: epithelium, stromal cells, T cells, macrophages, natural killer cells, and endothelium (Figures 1C, 1D, and S1B; Table S2).¹⁰ Every cell type was precisely identified across three tissue types, namely normal, eutopic and ectopic endometrium, and encompassing two menstrual cycles including proliferative and secretory phase (Figures 1E, 1F, and S1C). Altogether, our analysis yielded a comprehensive and high-precision catalog of endometrium from healthy controls and patients diagnosed with ovarian endometriosis.

Characterization of ciliated cells in endometriosis

After strict quality control, all epithelial cells with a median of 175,743 unique transcripts and 6,337 genes per cell were classified into four clusters based on their marker expression (Figures 2A, 2B, and S2A). Glandular proliferative cells, glandular secretory cells, and ciliated cells have been previously reported in healthy endometrium.¹¹ Ciliated and secretory cells were the two differentiated lineages with a common progenitor in the normal endometrium.¹¹ The majority of ectopic cells do not cluster with normal epithelial cells. Due to the high abundance of NNMT⁺ cells in this subset, we defined it as NNMT⁺ (Figures 2C and S2B).

To investigate preexisting alterations contributing to the disease, we compared glandular cells between eutopic and normal

tissues at the same phase (Figures 2D and S2C–S2E). Glandular proliferative cells in the eutopic endometrium at proliferative phase significantly upregulated genes involved in cilium assembly, such as *TPPP3*, *SNTN*, *C9orf24*, *TEKT1*, *RSPH1*, and *PIFO* (Figure 2D).^{12–16} Consistent with this finding, epithelial cells in the eutopic endometrium downregulated glandular secretory makers such as *SCGB2A1*, *HPGD*, and *ABCG1* (Figure 2D).¹¹ Through the construction of epithelial cell differentiation trajectories, we observed that a subset of glandular proliferative cells, characterized by an enhanced expression of ciliated genes, displayed an inclination toward differentiating into the ciliated lineage (Figures 2E–2H). The percentage of these cells within the eutopic endometrium exceeds that within the normal endometrium, potentially contributing to an increased proportion of ciliated cells in patients (Figures S2F and S2G).

In order to rigorously validate the increased proportions of ciliated cells, we performed immunohistochemistry (IHC) staining for two markers separately with different samples. *TPPP3* is a ciliated structure protein, and forkhead box protein J1 (FOXJ1) is a master regulator of the ciliated program.^{17,18} Compared to normal endometrium within the same phase, eutopic endometrium increased the percentage of both *TPPP3*⁺ and *FOXJ1*⁺ ciliated cells at the proliferative phase (Figures 3A, 3B, and S3A–S3C). These two ciliated markers, FOXJ1 and TPPP3, were co-expressed with another ciliary axoneme protein, acetylated α -tubulin (Figure 3C). It is also noteworthy that the percentage of ciliated cells was elevated in eutopic endometrium at the menstrual phase (Figure S3D). Taken together, we confirmed that eutopic endometrium from patients increased the percentage of ciliated cells, even in the shedding tissues.

In addition to the increased percentage of ciliated cells, we further investigated the defects present in these cells in endometriosis. Downregulation of *SULT1E1* (estrogen sulfotransferase) in the ciliated cells from eutopic endometrium was an interesting target (Figures 3D–3F, S3E, and S3F). *SULT1E1* catalyzes the sulfation of estradiol to inactivate it.¹⁹ Estradiol's principal role entails the promotion of cell proliferation and the inhibition of apoptosis through signaling pathways such as mitogen-activated protein kinase (MAPK) signaling pathways and the anti-apoptotic protein *BCL2*.^{20–22} Accordingly, decreased expression of *SULT1E1* in eutopic ciliated cells indicates a higher estradiol level, likely conferring survival advantages. Supporting this hypothesis, ciliated cells in patients upregulated anti-apoptotic genes including *BCL2* and key genes involved in the MAPK signaling pathway (*MEF2C*, *RAF1*), (Figure 3G).²³ Collectively, our results identified the abnormalities in ciliated cells of eutopic endometrium, which may resist apoptosis and enable their survival once they move to ectopic lesions.

To further explore the survival advantage of ciliated cells in the eutopic endometrium, we examined the proportion of ciliated

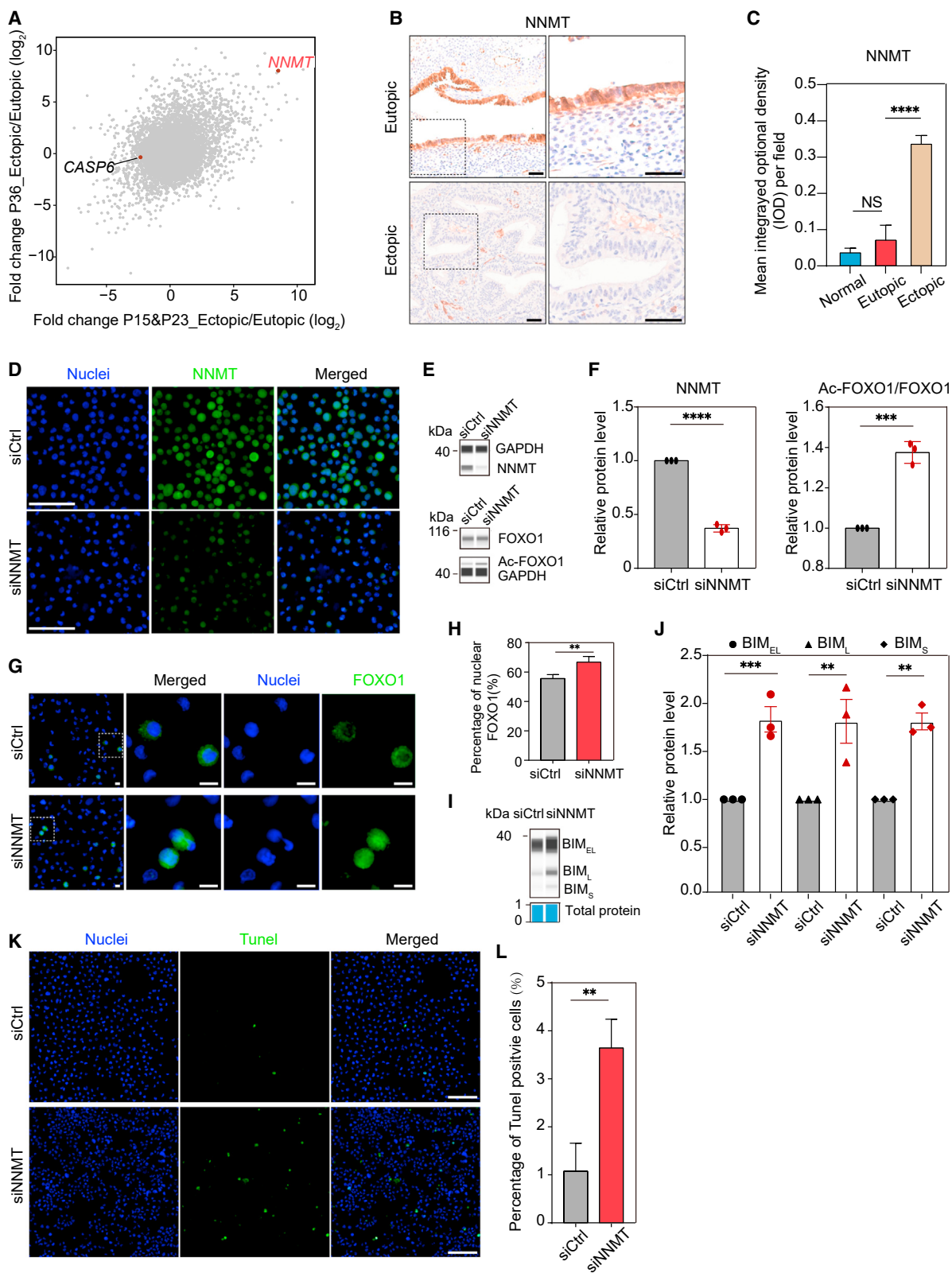
(G) Violin plot showing the increased expression of anti-apoptosis protein in eutopic ciliated cells. Wilcoxon rank-sum test. $p < 0.001$.

(H) Representative images of IHC staining for FOXJ1 (brown). Nuclei: blue. Close-up images (right) contain cells seen in the left black dashed box of the main image. Scale bar, 20 μ m

(I) Line chart showing the percentage of ciliated cells (FOXJ1⁺) in epithelial cells in 5 paired eutopic and ectopic tissue sections. Paired t test. * $p < 0.05$.

(J) Immunofluorescence staining showing the decreased expression of *SULT1E1* (green) in ectopic ciliated cells (FOXJ1, red) compared to the eutopic endometrium from the same patient. Nuclei: blue. Scale bar, 20 μ m.

See also Figures S3 and S4.



(legend on next page)

cells of the ectopic endometrium relative to the eutopic endometrium from the same patient. The proportion of ciliated cells in the ectopic epithelium was significantly higher (Figures 3H, 3I, and S4A). Moreover, the expression of SULT1E1 in ciliated cells was also decreased in ectopic lesions (Figures 3J and S4B). Altogether, these abnormalities in ciliated cells, including the increased proportion and reduced SULT1E1 expression, were observed in both the eutopic and ectopic endometrium. This shared pattern of abnormalities strongly suggested that ciliated cells demonstrated greater survival capabilities and may act as a potential origin of ectopic epithelium.

Inhibition of apoptosis mediated by NNMT in ectopic epithelium

Resistance to apoptosis has been identified in ectopic lesions supported by reduced TUNEL staining, but the underlying mechanism remains elusive.²⁴ To find other target genes regulating the apoptosis, we compared the epithelial cells in ectopic lesions with the total epithelial cells from paired eutopic endometrium to mitigate individual and phase biases. Interestingly, we found that epithelial cells in ectopic lesions overexpressed *NNMT* and downregulated the cysteine protease *CASP6*, an executor caspase of apoptosis (Figure 4A). The overexpression of *NNMT* was further validated through IHC (Figures 4B, 4C, and S4C). *NNMT* enhances the stability of *SIRT1* deacetylase, which subsequently leads to the downregulation of *FOXO1*'s transcriptional activity through deacetylation.^{25–27} Acetylation of *FOXO1* is known to regulate its nuclear localization and subsequently influence its transcriptional activity.^{28,29} In the endometrial epithelial cells, the nuclear localization of *FOXO1* plays important roles in inducing apoptosis and embryo invasion.³⁰ Based on these findings, we postulated *NNMT* as a target implicated in the reduced apoptosis of epithelial cells. To confirm this, we performed *NNMT* knockdown experiments in the endometriotic cell line 12Z and observed an increase in acetylated *FOXO1* expression, while the total *FOXO1* expression remained unchanged (Figures 4D–4F). Given that *FOXO1* primarily exerts its transcriptional activity when localized in the nucleus,³¹ we stained *FOXO1* following *NNMT* knockdown and observed

enhanced nuclear localization (Figures 4G and 4H). We next examined the expression of *FOXO1*-target gene *BIM*, a key pro-apoptotic member of the BCL-2 family of proteins.³² *BIMS* is the most cytotoxic isoform and is expressed during apoptosis. The *BIMEL* and *BIML* isoforms are released from the dynein motor complex during apoptosis. Remarkably, *NNMT* knockdown in the 12Z cell line led to increased expression of all three *BIM* isoforms (Figures 4I and 4J). Consistent with the upregulation of *BIM*, the proportion of TUNEL⁺ cells is increased, further confirming enhanced cell apoptosis mediated by *NNMT* knockdown (Figures 4K and 4L). Correspondingly, in ectopic endometrium, *NNMT*[−] cells are more prone to apoptosis, aligning with our *in vitro* findings (Figure S4D). Altogether, our data demonstrated that *NNMT* knockdown promoted the acetylation and nuclear accumulation of *FOXO1*, thereby elevating *BIM* expression and inducing apoptosis. These findings suggested that *NNMT* is a potential therapeutic target for modulating cell apoptosis in ectopic lesions.

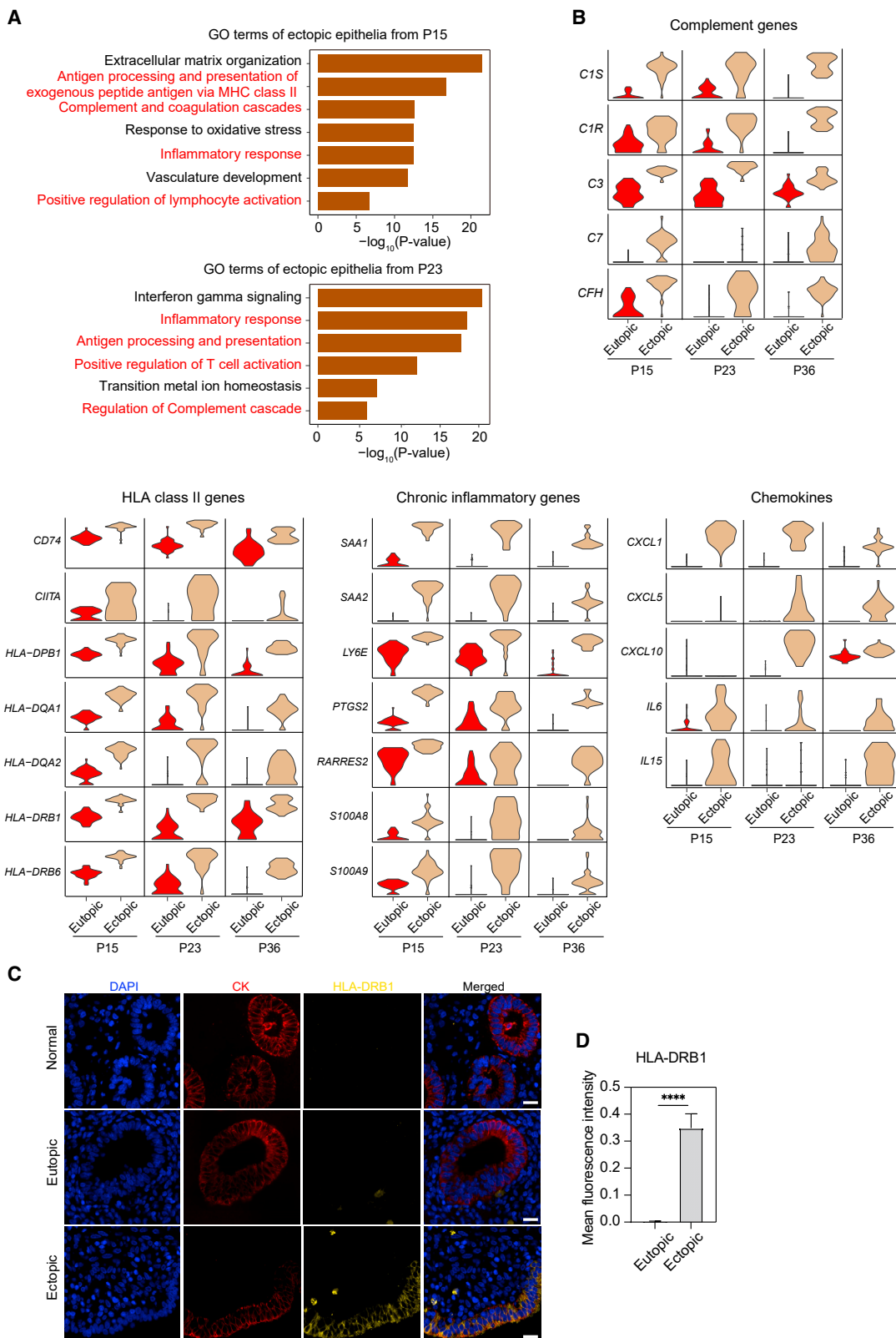
An epithelial-immune dual feature of ectopic epithelium

Compared to matched epithelial cells from eutopic endometrium in the same patient, ectopic epithelium exhibited a distinct enrichment of immune-related features. This included the upregulation of genes involved in antigen processing and presentation of exogenous peptide antigen via HLA class II (e.g., *HLA-DRB1*, *HLA-DRB6*, *HLA-DQB1*, *HLA-DPB1*), complement and coagulation cascades (e.g., *C1QC*, *C3*, *C7*), the inflammatory response (e.g., *LY6E*, *PTGS2*, *SAA1*), and positive regulation of lymphocyte activation (e.g., *CXCL1*, *CXCL5*, *CXCL10*, *IL6*) (Figures 5A, 5B, S5A, and S5B; Table S3). Under normal conditions, these HLA class II genes, complement genes, and chemokines are specifically expressed in immune cells and are involved in immune cell recruitment, activation, and differentiation. Immunohistochemical staining of normal, eutopic, and ectopic endometrium confirmed the overexpressed *HLA-DRB1* of epithelial cells in ectopic lesions (Figures 5C, 5D, and S5C). Together, these data highlighted the dual epithelial-immune feature of ectopic epithelial cells in endometriosis and suggested their immunoregulatory role in the disease.

Figure 4. Knockdown of NNMT induces apoptosis of endometriotic cells via the acetylation of FOXO1 and nuclear localization

- (A) Volcano plot comparing ectopic to matching eutopic epithelial cells from 3 patients.
- (B) IHC staining for *NNMT*. Close-up images (right) contain cells seen in the left black dashed box of the main image. Scale bar, 50 µm
- (C) Bar plot showing the mean integral optical density of *NNMT* in epithelial cells per field. Normal: 7 tissue sections; eutopic: 8 tissue sections; ectopic: 10 tissue sections. Data are represented as mean with SEM. Mann-Whitney test was used to derive p values. ***p < 0.0001. NS means no significance.
- (D) Immunofluorescence staining showing reduced expression of *NNMT* (green) in endometriotic cell line 12Z cells. Scale bar, 100 µm
- (E) Immunoblot of *NNMT*, *FOXO1*, and acetylated *FOXO1* in 12Z cell line.
- (F) Bar plots showing the expression of *NNMT* relative to *GAPDH* (left) and acetylated *FOXO1* relative to *FOXO1* (right) in 12Z cell lines. Data are represented as mean with SEM. Two-tailed t test, ***p < 0.0001. n = 3 replicates. **p < 0.001.
- (G) Immunofluorescence staining showing increased nuclear localization of *FOXO1* (green) in endometriotic cell line 12Z cells. Close-up images (right) contain cells seen in the left dashed box of the merged image. Scale bar, 10 µm
- (H) Bar plot showing the percentage of nuclear *FOXO1* relative to the *FOXO1*⁺ cells. Data are represented as mean with SEM. siCtrl: n = 9 fields (1 mm² per field). siNNMT: n = 9 fields (1 mm² per field). Two-tailed t test, **p < 0.01.
- (I) Immunoblot of three isoforms of *BIM* upon knockdown of *NNMT* in 12Z cells.
- (J) Bar plot showing the expression of *BIM* relative to total protein in 12Z cells. Data are represented as mean with SEM. n = 3 replicates. Two-tailed t test, ***p < 0.001 and **p < 0.01.
- (K) Immunofluorescence staining showing the TUNEL staining. Damaged DNA (apoptotic cells) are colored green. Scale bar, 100 µm
- (L) Bar plots showing the percentage of apoptotic cells in 12Z cells. Data are represented as mean with SEM. Mann-Whitney test was used, n = 15 random fields from 3 replicates in each group. **p < 0.01.

See also Figure S4.



(legend on next page)

Immunoregulatory roles of epithelial cells in ectopic lesions

T cells from all samples were classified into 7 subtypes based on the expression of well-known marker genes (Figures 6A, 6B, and S6A). To assess the states of T cells, we utilized the IFN- γ expression signatures as an indicator of activation (Figure 6C; Table S4). A higher score indicated a more activated state in ectopic T cells. To explore whether epithelial cells with epithelial-immune dual features play roles in immunoregulation by regulating T cell response, we performed ligand-receptor interaction analysis. In ectopic lesions, epithelial cells and T cells showed stronger interactions, including CXCL10-CXCR3, interleukin-15 (IL-15)-IL-15 receptor, and (Tenascin-C) TNC-a4b1 complex (Figure 6D). These interactions suggested that chemokines secreted by epithelial cells in ectopic lesions were responsible for the recruitment of T cells.

We next confirmed that epithelial cells mediated the infiltration of T cells. Immunofluorescence staining of ectopic endometrium showed an increased density of infiltrated CD3 $^{+}$ T cells surrounding HLA-DRB1 $^{\text{high}}$ epithelial cells (Figures S6B and S6C). Among these infiltrated T cells, we further examined the T cell subtypes in ectopic endometrium. Within a distance of 20 μm from HLA-DRB1 $^{\text{high}}$ epithelial cells, the density of CD4 $^{+}$ T cells was higher, while the percentage of CD4 $^{+}$ FOXP3 $^{+}$ Treg cells (regulatory T cells) was decreased (Figures 6E–6G and S6D). Treg cells are essential for limiting chronic inflammatory diseases by reducing the self-reactivity of immune cells and excessive inflammation. The higher proportion of CD4 $^{+}$ T cells and the lower proportion of Treg cells suggested that HLA class II $^{+}$ epithelial cells recruited T cells and potentially stimulated the inflammatory response of T cells in ectopic lesions.

HLA class II genes expressed in macrophages are involved in presenting antigens and stimulating or inhibiting CD4 $^{+}$ T cell rather than CD8 $^{+}$ T cell response. Previous studies found that several tumor cells expressed HLA class II, but whether they stimulated or inhibited T cells was not fully understood.^{33–35} In this study, to further investigate whether HLA class II $^{+}$ epithelial cells directly stimulate T cells, we performed a co-culture experiment using the endometriotic cell line 12Z and T cells (Figure 6H). 12Z cell lines were firstly stimulated to express the HLA class II complex (Figures S6F and S6G). After co-culturing with T cells, HLA class II $^{+}$ epithelial cells stimulated the activation of CD4 $^{+}$ T cells while not stimulating CD8 $^{+}$ T cells (Figures 6I and S6H). Together, HLA class II $^{+}$ epithelial cells in ectopic lesions directly stimulated CD4 $^{+}$

T cells through HLA class II. These data suggested that epithelial cells were directly involved in the inflammatory response and disrupted immune homeostasis in ectopic lesions.

The alterations of stromal cells in endometriosis

The stromal cells, with a median of 113,312 unique transcripts and 5,013 genes per cell, were clustered and classified into endometrial stroma proliferative, endometrial stroma secretory, and ovarian stroma based on marker expression (Figures 7A–7C). Compared to normal stromal cells, eutopic endometrial stroma at proliferative phase significantly upregulated 576 genes and downregulated 334 genes (false discovery rate < 0.05, $\log_2[\text{fold change}] > 0.25$; Table S5). The upregulated genes were enriched in biological function and processes such as positive regulation of MAPK cascade (ATF4, MAP2K1, MEF2C, PIK3C2A, JUND, and JUN) and response to insulin (IGF1R, IGF2R, IRS2, and SHC2) (Figures 7D and 7E). The signal transduction of insulin growth factors (IGFs) on the growth axis is mainly through the activation of the MAPK kinase activation pathway, which transmits mitotic and metabolic signals to the nucleus of the cells, thereby initiating the secretion of IGFs, promoting cell proliferation and inhibiting cell apoptosis.³⁶ These elevated pro-survival signals in stromal cells from patients likely contribute to their survival in the ectopic lesions.

DISCUSSION

Our single-cell transcriptomic analysis encompasses 34 samples from both healthy individuals and women with ovarian endometriosis and further highlights the critical roles of epithelial cells in the pathophysiology of endometriosis. Our atlas offers significant advantages for a comprehensive investigation of endometriosis. This study has generated a higher-resolution RNA landscape compared to previous atlases, facilitating the identification of more accurate cellular states.^{7,8} Furthermore, normal and eutopic tissues are challenging to obtain and thus have been underrepresented in previous studies. By obtaining normal and eutopic endometrium during identical phases, we have effectively minimized phase-related differences, allowing us to pinpoint causal abnormalities in eutopic endometrium. Finally, our study successfully compares ectopic cells with eutopic cells from the same patients. This approach enhances the precision of our findings by controlling for both phase and individual variability.

Figure 5. An epithelial-immune dual feature of ectopic epithelial cells

(A) Biological processes enriched in ectopic upregulated genes compared to matching eutopic epithelial cells in patients 15 and 23. Significantly discriminatory genes of ectopic epithelium relative to eutopic epithelium in patients 15 and 23 were used as input for GO enrichment analysis (FDR < 0.05, $\log_2[\text{fold change}] > 0.25$). The terms related to immune response are colored red.

(B) Violin plots showing upregulated expression of immune related genes in paired ectopic and eutopic epithelial cells from 3 patients (FDR < 0.05, $\log_2[\text{fold change}] > 0.25$).

(C) Immunofluorescence staining of epithelial cells marker (pan-CK) and HLA-DRB1. Representative images of endometrial epithelial glands in proliferative phase. CK and HLA-DRB1 antibody stainings are colored by red and yellow, respectively and nuclei blue. Scale bar, 20 μm .

(D) Integrated fluorescence intensity of HLA-DRB1 antibody from all images of epithelial cells. 10 eutopic and 11 ectopic tissue sections are included. 6–15 fields are randomly selected in one section. Data are represented as mean with SEM. Two-tailed t test, ***p < 0.0001.

See also Figure S5.

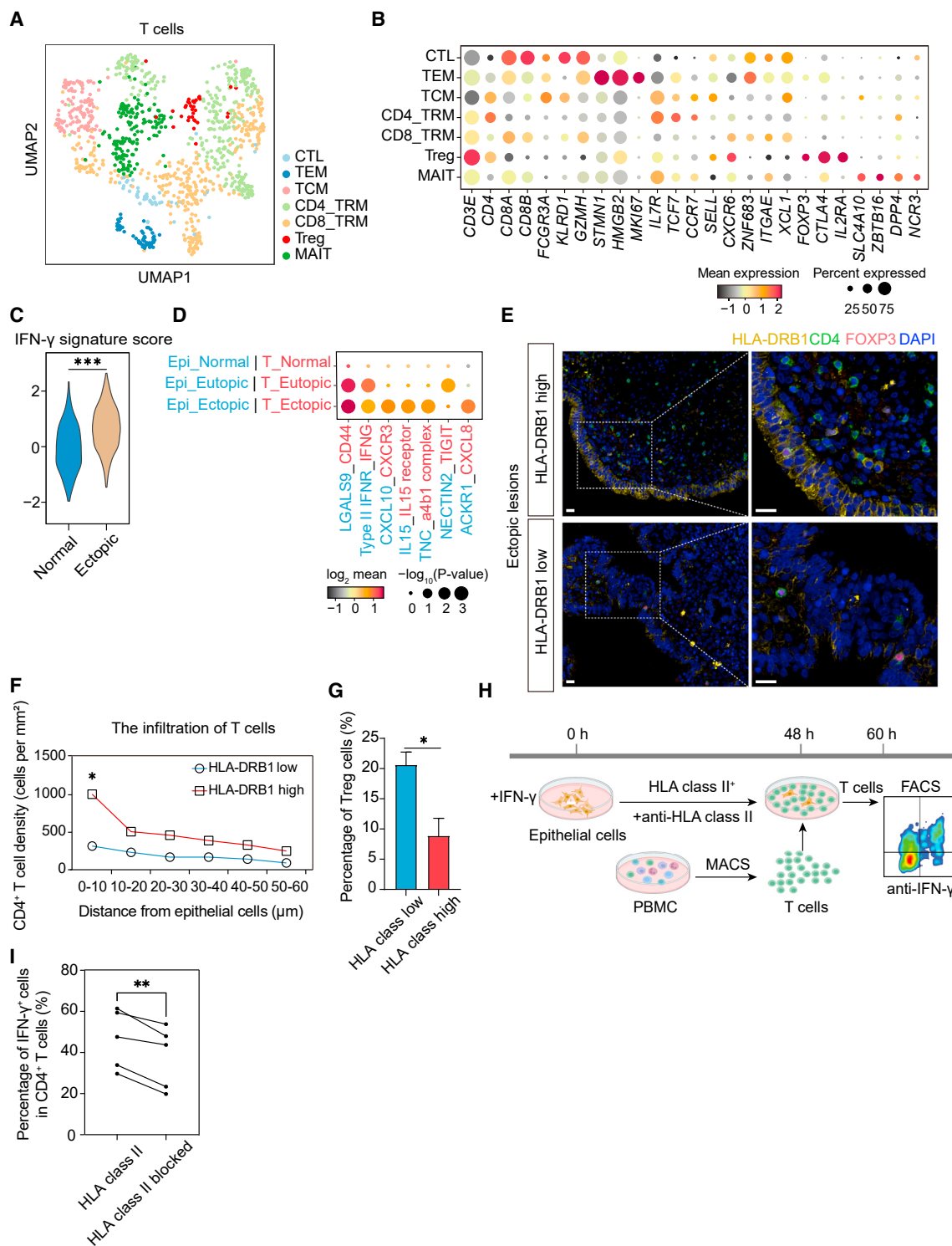


Figure 6. The regulatory roles of ectopic epithelial cells in T cell states

(A) UMAP of subclustered T cells from all individuals.

(B) Dot plot showing the Z score-scaled mean expression of marker genes.

(C) Violin plot showing the IFN- γ signature score of T cells (Table S4). Wilcoxon rank-sum test. ***p < 0.001.

(D) Dot plot showing selected ligand-receptor interactions (permutation test, p < 0.05) between epithelial cells and T cells. The color of the dot represents the log2-transformed mean expression level.

(legend continued on next page)

Previous studies have indicated important molecular abnormalities in the eutopic endometrium.^{37–40} However, there remains a lack of detailed understanding of which epithelial cell populations and what specific alterations are correlated to the formation of endometriotic lesions. Here, we identify an increased proportion of ciliated cells in both eutopic and ectopic endometrium, characterized by a reduced expression of SULT1E1 (Figure 7F). Our success in discovering the defects of ciliated cells is due to the comparison of eutopic and normal endometrium within the same menstrual phase, coupled with our high-resolution gene detection in individual cells. The diminished expression of SULT1E1, previously associated with increased estrogen availability in endometrial and breast cancers, may confer a survival advantage to ciliated cells in endometriosis and thereby lead to their increased proportions (Figure 7F).^{41–43} Further functional studies are essential to ascertain whether abnormal ciliated cells play a role in the onset of endometriosis and whether they possess the capacity to trans-differentiate into both ciliated and non-ciliated cell types within ectopic lesions, similar to cellular differentiation patterns observed in ovarian and endometrial cancers.^{44–46}

Apoptosis is markedly attenuated in endometriotic epithelial cells as indicated in previous researches.^{24,47} Our study has identified NNMT as a key gene involved in inhibiting apoptosis through the FOXO1 pathway in ectopic epithelium (Figure 7F). As an FDA-approved drug target, small-molecule inhibitors of NNMT have been investigated for their therapeutic potential in treating conditions like cancer and diabetes.⁴⁸ This discovery underscores the importance of NNMT as a vital target for modulating apoptosis in endometriosis therapy.

In endometriosis, cytokine production and immune cell infiltration have been linked to immune cell dysfunction.⁴⁹ Our study unveils a significant aspect of endometriosis-associated inflammation. We demonstrate that epithelial cells in ectopic lesions actively contribute to an imbalanced inflammatory response by secreting chemokines and stimulating T cells through the HLA class II complex (Figure 7F). The activation of T cells increases IFN- γ production, which could in turn induce the expression of HLA class II genes in epithelial cells, thereby establishing a feedback cycle that sustains chronic inflammation in ectopic lesions.⁵⁰ The chronic antigen stimulation by epithelial cells not only leads to inflammation but may also contribute to T cell exhaustion and thus impairs the clearance of ectopic tissues.⁵¹ This finding provides clues for mitigating inflammation related damage in endometriosis.

(E) Immunofluorescence staining of ectopic endometrium. Close-up images (right) contain T cells seen in the left white dashed box of the main image. The top images were referred as epithelial cells with higher expression of HLA-DRB1. Scale bar, 20 μ m.

(F) Line graph showing the density of T cells in ectopic sections. T cells were categorized into six groups based on their distance from the epithelial layer, with each group representing a 10 μ m increment. 3 HLA-DRB1^{high} fields derived from 3 ectopic sections and 4 HLA-DRB1^{low} fields from 4 ectopic sections are included. Two-tailed t test, *p < 0.05.

(G) Bar chart showing the percentage of CD4⁺ FOXP3⁺ Treg cells at a distance of 20 μ m from epithelial layer in ectopic sections. HLA-DRB1^{high} fields selected from 3 ectopic sections and HLA-DRB1^{low} fields from 3 ectopic sections were included in the analysis. Data are represented as mean with SEM. Two-tailed t test, *p < 0.05.

(H) Schematic of processing of epithelial cell and T cell co-culture experiments. Endometriotic cell line 12Z was used. Anti-HLA class II means HLA class II⁺ epithelial cells were blocked by anti-HLA class II antibody. IFN- γ antibody were used to analyze the activation of T cells. MACS means magnetic-activated cell sorting for CD3⁺ T cells. FACS means fluorescence-activated cell sorting for T cells.

(I) Line chart showing the percentage of activated T cells (IFN- γ ⁺) relative to CD4⁺ T cells after co-culture with endometriotic cell line 12Z. n = 5 replicates. Paired t test. **p < 0.01.

See also Figure S6.

Limitations of the study

While our high-resolution atlas yields insights into the pathology of endometriosis, it is constrained by a relatively low cell count, limiting our ability to identify a wider range of cell subtypes related to the disease. The transcriptomic profile of ectopic epithelium is predominantly derived from three patients, emphasizing the necessity of experimental validation of these genetic features with more diverse samples. Additionally, our findings are specifically related to ovarian endometriosis, and caution should be exercised when extrapolating these results to other endometriosis types. Moreover, the underrepresentation of tissues from the mid- and late-secretory phases, as well as the menstrual phase, may lead to the omission of significant phase-specific insights. The shedding endometrium during retrograde menstruation could be key in understanding the cause of endometriosis. Future studies should broaden the sample size and encompass more disease and menstrual stages to enhance the comprehensiveness of the understanding.

STAR★METHODS

Detailed methods are provided in the online version of this paper and include the following:

- [KEY RESOURCES TABLE](#)
- [RESOURCE AVAILABILITY](#)
 - Lead contact
 - Materials availability
 - Data and code availability
- [EXPERIMENTAL MODEL AND STUDY PARTICIPANT DETAILS](#)
 - Human participants
 - Cell culture
- [METHOD DETAILS](#)
 - Dissociation of tissue and flow cytometry
 - Single-cell RNA-seq library construction
 - Analysis of single cell RNA-Seq data
 - Cell interaction analysis
 - IFN- γ signature scoring
 - Immunohistochemistry
 - Immunofluorescence staining of FFPE tissue
 - NNMT knockdown by siRNA
 - Immunoblots
 - TUNEL staining
 - Co-culture assay

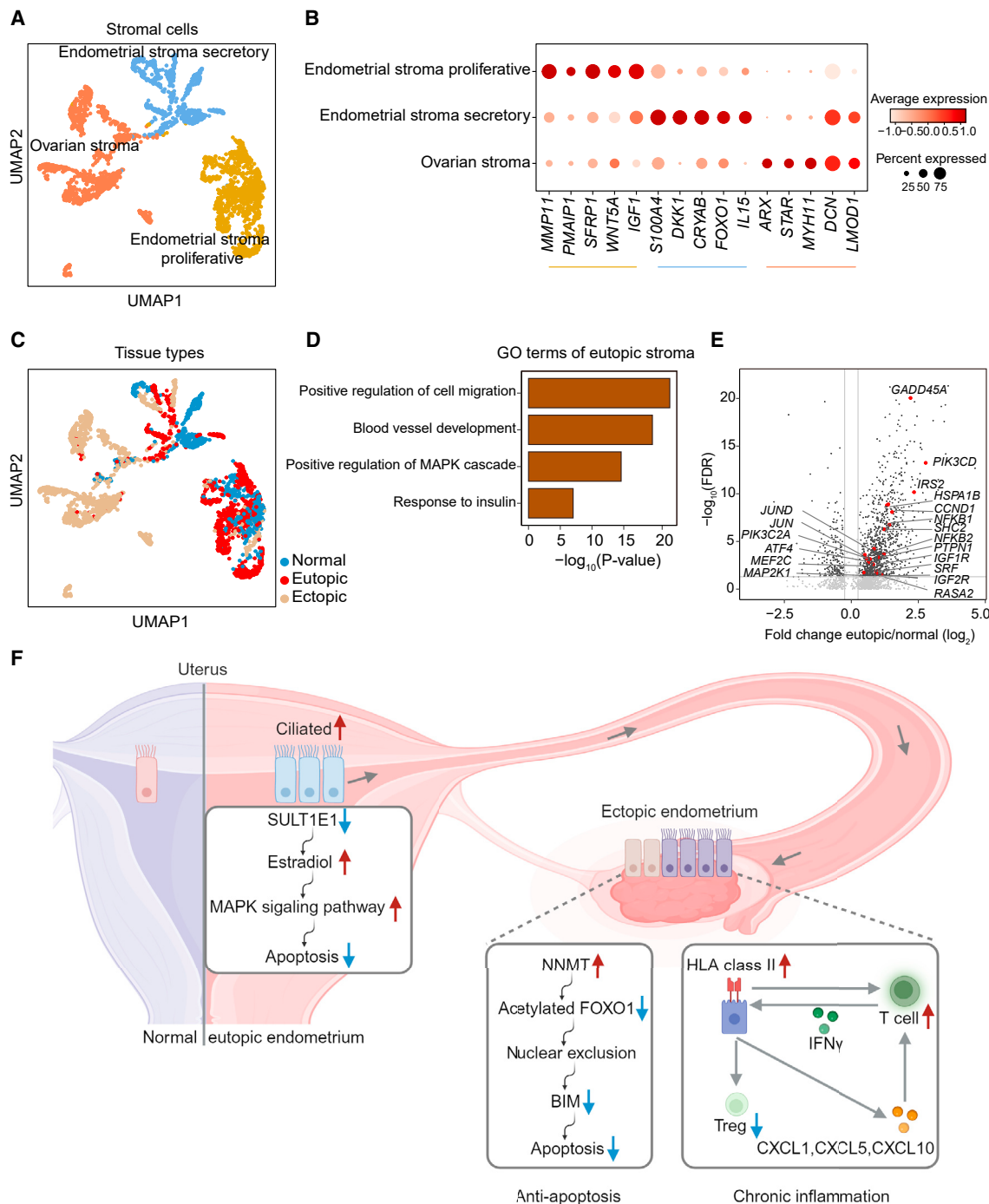


Figure 7. Alterations of eutopic stromal cells and proposed illustration for pathogenesis of endometriosis

- (A) UMAP of subclustered stromal populations from all individuals including both proliferative and secretory phases.
- (B) Dot plot showing the Z score-scaled mean expression of genes characteristic of each stromal subset. The line under the genes represents the cell types in order of endometrial stroma proliferative, endometrial stroma secretory, and ovarian stroma.
- (C) UMAP representations colored by sampling sites.
- (D) Biological processes enriched in eutopic upregulated genes relative to normal stromal cells at proliferative phase.
- (E) Volcano plots comparing eutopic to normal stromal cells from 7 patients and 5 normal individuals at proliferative phase. Significantly discriminatory genes ($\text{FDR} < 0.05$, $\log_2[\text{fold change}] > 0.25$) are colored in black, and genes described in the results are colored in red.
- (F) Schematic illustrating the proposed pathogenesis of ovary endometriosis. Compared to normal endometrium, eutopic and ectopic endometria exhibit common alterations. Both eutopic and ectopic endometria increase the percentage of ciliated cells, which may resist the apoptosis of shedding tissue mediated

(legend continued on next page)

- Flow cytometry
- **QUANTIFICATION AND STATISTICAL ANALYSIS**
- Data analysis of sequencing data
- Experimental data analysis

SUPPLEMENTAL INFORMATION

Supplemental information can be found online at <https://doi.org/10.1016/j.celrep.2024.113716>.

ACKNOWLEDGMENTS

All schematic panels were created using [Biorender.com](#). This work was funded by the National Natural Science Foundation of China (grant no. 81971360) and the National Key Research and Development Program (grant no. 2022YFC2704001).

AUTHOR CONTRIBUTIONS

F.T., X.C., J.Y., and X.Z. designed the project. J.Y., L.Z., and E.C. carried out the experiments. M.L. and X.Z. performed the bioinformatics analysis. J.Y. and M.L. interpreted the experimental and bioinformatics results and wrote the manuscript. X.X., H.Z., T.C., H.C., J.L., S.W., and L.D. contributed to sample collection and the manuscript by providing valuable advice. F.T. and X.C. revised the manuscript.

DECLARATION OF INTERESTS

The authors declare no competing interests.

Received: July 12, 2023

Revised: November 19, 2023

Accepted: January 11, 2024

Published: February 26, 2024

REFERENCES

1. Critchley, H.O.D., Maybin, J.A., Armstrong, G.M., and Williams, A.R.W. (2020). Physiology of the Endometrium and Regulation of Menstruation. *Physiol. Rev.* 100, 1149–1179. <https://doi.org/10.1152/physrev.00031.2019>.
2. Noyes, R.W., Hertig, A.T., and Rock, J. (1950). Dating the Endometrial Biopsy. *Fertil. Steril.* 1, 3–25. [https://doi.org/10.1016/s0015-0282\(16\)30062-0](https://doi.org/10.1016/s0015-0282(16)30062-0).
3. Chapron, C., Fauconnier, A., Vieira, M., Barakat, H., Dousset, B., Pansini, V., Vacher-Lavenu, M.C., and Dubuisson, J.B. (2003). Anatomical distribution of deeply infiltrating endometriosis: surgical implications and proposition for a classification. *Hum. Reprod.* 18, 157–161. <https://doi.org/10.1093/humrep/deg009>.
4. Zondervan, K.T., Becker, C.M., and Missmer, S.A. (2020). Endometriosis. *N. Engl. J. Med.* 382, 1244–1256. <https://doi.org/10.1056/NEJMra1810764>.
5. Nirgianakis, K., Ma, L., McKinnon, B., and Mueller, M.D. (2020). Recurrence Patterns after Surgery in Patients with Different Endometriosis Subtypes: A Long-Term Hospital-Based Cohort Study. *J. Clin. Med.* 9, 496. <https://doi.org/10.3390/jcm9020496>.
6. Ma, J., Zhang, L., Zhan, H., Mo, Y., Ren, Z., Shao, A., and Lin, J. (2021). Single-cell transcriptomic analysis of endometriosis provides insights into fibroblast fates and immune cell heterogeneity. *Cell Biosci.* 11, 125. <https://doi.org/10.1186/s13578-021-00637-x>.
7. Tan, Y., Flynn, W.F., Sivajothi, S., Luo, D., Bozal, S.B., Davé, M., Luciano, A.A., Robson, P., Luciano, D.E., and Courtois, E.T. (2022). Single-cell analysis of endometriosis reveals a coordinated transcriptional programme driving immunotolerance and angiogenesis across eutopic and ectopic tissues (vol 24, pg 1306, 2022). *Nat. Cell Biol.* 24, 1679. <https://doi.org/10.1038/s41556-022-01023-6>.
8. Fonseca, M.A.S., Haro, M., Wright, K.N., Lin, X., Abbasi, F., Sun, J., Hernandez, L., Orr, N.L., Hong, J., Choi-Kuea, Y., et al. (2023). Single-cell transcriptomic analysis of endometriosis. *Nat. Genet.* 55, 255–267. <https://doi.org/10.1038/s41588-022-01254-1>.
9. Ferenczy, A., and Bergeron, C. (1991). Histology of the human endometrium: from birth to senescence. *Ann. N. Y. Acad. Sci.* 622, 6–27. <https://doi.org/10.1111/j.1749-6632.1991.tb37847.x>.
10. Wang, W., Vilella, F., Alama, P., Moreno, I., Mignardi, M., Isakova, A., Pan, W., Simon, C., and Quake, S.R. (2020). Single-cell transcriptomic atlas of the human endometrium during the menstrual cycle. *Nat. Med.* 26, 1644–1653. <https://doi.org/10.1038/s41591-020-1040-z>.
11. Garcia-Alonso, L., Handfield, L.F., Roberts, K., Nikolakopoulou, K., Fernando, R.C., Gardner, L., Woodhams, B., Arutyunyan, A., Polanski, K., Hoo, R., et al. (2021). Mapping the temporal and spatial dynamics of the human endometrium *in vivo* and *in vitro*. *Nat. Genet.* 53, 1698–1711. <https://doi.org/10.1038/s41588-021-00972-2>.
12. Ryan, R., Failler, M., Reilly, M.L., Garfa-Traore, M., Delous, M., Filhol, E., Reboul, T., Bole-Feysot, C., Nitschke, P., Baudouin, V., et al. (2018). Functional characterization of tektin-1 in motile cilia and evidence for TEKT1 as a new candidate gene for motile ciliopathies. *Hum. Mol. Genet.* 27, 266–282. <https://doi.org/10.1093/hmg/ddx396>.
13. Kott, E., Legendre, M., Copin, B., Papon, J.F., Dastot-Le Moal, F., Montantin, G., Duquesnoy, P., Piterboth, W., Amram, D., Bassinet, L., et al. (2013). Loss-of-function mutations in RSPH1 cause primary ciliary dyskinesia with central-complex and radial-spoke defects. *Am. J. Hum. Genet.* 93, 561–570. <https://doi.org/10.1016/j.ajhg.2013.07.013>.
14. Kinzel, D., Boldt, K., Davis, E.E., Burtscher, I., Trümbach, D., Diplas, B., Attié-Bitach, T., Wurst, W., Katsanis, N., Ueffing, M., and Lickert, H. (2010). Pitchfork Regulates Primary Cilia Disassembly and Left-Right Asymmetry. *Dev. Cell* 19, 66–77. <https://doi.org/10.1016/j.devcel.2010.06.005>.
15. Pedersen, L.B., Schröder, J.M., Satir, P., and Christensen, S.T. (2012). The Ciliary Cytoskeleton. *Compr. Physiol.* 2, 779–803. <https://doi.org/10.1002/cphy.c110043>.
16. Patir, A., Fraser, A.M., Barnett, M.W., McTeir, L., Rainger, J., Davey, M.G., and Freeman, T.C. (2020). The transcriptional signature associated with human motile cilia. *Sci. Rep.* 10, 10814. <https://doi.org/10.1038/s41598-020-66453-4>.
17. Orosz, F., and Ovádi, J. (2008). TPPP orthologs are ciliary proteins. *FEBS Lett.* 582, 3757–3764. <https://doi.org/10.1016/j.febslet.2008.10.011>.
18. Yu, X., Ng, C.P., Habacher, H., and Roy, S. (2008). Foxj1 transcription factors are master regulators of the motile ciliogenic program. *Nat. Genet.* 40, 1445–1453. <https://doi.org/10.1038/ng.263>.
19. Rizner, T.L. (2016). The Important Roles of Steroid Sulfatase and Sulfo-transferases in Gynecological Diseases. *Front. Pharmacol.* 7, 30. <https://doi.org/10.3389/fphar.2016.00030>.
20. Chimento, A., De Luca, A., Avena, P., De Amicis, F., Casaburi, I., Sirianni, R., and Pezzi, V. (2022). Estrogen Receptors-Mediated Apoptosis in Hormone-Dependent Cancers. *Int. J. Mol. Sci.* 23, 1242.

by increased estradiol and the downstream MAPK signaling pathway. Shedding endometrial cells retrograde into the ovary through the fallopian tube (gray arrow). After translocating into ectopic lesions, ectopic epithelial cells increase the expression of NNMT, which downregulates the acetylation of FOXO1. The deacetylation of FOXO1 contributes to the nuclear exclusion of FOXO1 and thus the decreased expression of pro-apoptotic protein BIM. Ectopic epithelial cells also recruit and stimulate T cells via both chemokines and HLA class II, whereas HLA class II⁺ epithelial cells inhibit the infiltration of Treg cells. The activated T cells secrete more IFN-γ, which contributes to the expression of HLA class II in epithelium and chronic inflammation in ectopic lesions. Created with [Biorender.com](#).

21. Marino, M., and Ascenzi, P. (2008). Membrane association of estrogen receptor α and β influences 17 β -estradiol-mediated cancer cell proliferation. *Steroids* 73, 853–858. <https://doi.org/10.1016/j.steroids.2007.12.003>.
22. Dawson, S.J., Makretsov, N., Blows, F.M., Driver, K.E., Provenzano, E., Le Quesne, J., Baglietto, L., Severi, G., Giles, G.G., McLean, C.A., et al. (2010). BCL2 in breast cancer: a favourable prognostic marker across molecular subtypes and independent of adjuvant therapy received (vol 103, pg 668, 2010). *Br. J. Cancer* 103, 1137. <https://doi.org/10.1038/sj.bjc.6605921>.
23. Zhang, W., and Liu, H.T. (2002). MAPK signal pathways in the regulation of cell proliferation in mammalian cells. *Cell Res.* 12, 9–18. <https://doi.org/10.1038/sj.cr.7290105>.
24. Béliard, A., Noël, A., and Foidart, J.M. (2004). Reduction of apoptosis and proliferation in endometriosis. *Fertil. Steril.* 82, 80–85. <https://doi.org/10.1016/j.fertnstert.2003.11.048>.
25. Hong, S., Moreno-Navarrete, J.M., Wei, X., Kikukawa, Y., Tzameli, I., Prasad, D., Lee, Y., Asara, J.M., Fernandez-Real, J.M., Maratos-Flier, E., and Pissios, P. (2015). Nicotinamide N-methyltransferase regulates hepatic nutrient metabolism through Sirt1 protein stabilization. *Nat. Med.* 21, 887–894. <https://doi.org/10.1038/nm.3882>.
26. Yang, Y., Zhao, Y., Liao, W., Yang, J., Wu, L., Zheng, Z., Yu, Y., Zhou, W., Li, L., Feng, J., et al. (2009). Acetylation of FoxO1 Activates Bim Expression to Induce Apoptosis in Response to Histone Deacetylase Inhibitor Depsiteptide Treatment. *Neoplasia* 11, 313–324. <https://doi.org/10.1593/neo.81358>.
27. Greer, E.L., and Brunet, A. (2005). FOXO transcription factors at the interface between longevity and tumor suppression. *Oncogene* 24, 7410–7425. <https://doi.org/10.1038/sj.onc.1209086>.
28. Senf, S.M., Sandesara, P.B., Reed, S.A., and Judge, A.R. (2011). p300 Acetyltransferase activity differentially regulates the localization and activity of the FOXO homologues in skeletal muscle. *Am. J. Physiol. Cell Physiol.* 300, C1490–C1501. <https://doi.org/10.1152/ajpcell.00255.2010>.
29. Zhang, M., Zhang, Q., Hu, Y., Xu, L., Jiang, Y., Zhang, C., Ding, L., Jiang, R., Sun, J., Sun, H., and Yan, G. (2017). miR-181a increases FoxO1 acetylation and promotes granulosa cell apoptosis via SIRT1 downregulation. *Cell Death Dis.* 8, e3088. <https://doi.org/10.1038/cddis.2017.467>.
30. Vasquez, Y.M., Wang, X., Wetendorf, M., Franco, H.L., Mo, Q., Wang, T., Lanz, R.B., Young, S.L., Lessey, B.A., Spencer, T.E., et al. (2018). FOXO1 regulates uterine epithelial integrity and progesterone receptor expression critical for embryo implantation. *PLoS Genet.* 14, e1007787. <https://doi.org/10.1371/journal.pgen.1007787>.
31. Kawamori, D., Kaneto, H., Nakatani, Y., Matsuoka, T.A., Matsuhashi, M., Hori, M., and Yamasaki, Y. (2006). The forkhead transcription factor foxo1 bridges the JNK pathway and the transcription factor PDX-1 through its intracellular translocation. *J. Biol. Chem.* 281, 1091–1098. <https://doi.org/10.1074/jbc.M508510200>.
32. Gilley, J., Coffer, P.J., and Ham, J. (2003). FOXO transcription factors directly activate bim gene expression and promote apoptosis in sympathetic neurons. *J. Cell Biol.* 162, 613–622. <https://doi.org/10.1083/jcb.200303026>.
33. Forero, A., Li, Y., Chen, D., Grizzle, W.E., Updike, K.L., Merz, N.D., Down-Kelly, E., Burwell, T.C., Vaklavas, C., Buchsbaum, D.J., et al. (2016). Expression of the MHC Class II Pathway in Triple-Negative Breast Cancer Tumor Cells Is Associated with a Good Prognosis and Infiltrating Lymphocytes. *Cancer Immunol. Res.* 4, 390–399. <https://doi.org/10.1158/2326-6066.CIR-15-0243>.
34. McCaw, T.R., Li, M., Starenki, D., Cooper, S.J., Liu, M., Meza-Perez, S., Arend, R.C., Buchsbaum, D.J., Forero, A., and Randall, T.D. (2019). The expression of MHC class II molecules on murine breast tumors delays T-cell exhaustion, expands the T-cell repertoire, and slows tumor growth. *Cancer Immunol. Immunol.* 68, 175–188. <https://doi.org/10.1007/s00262-018-2262-5>.
35. Sconocchia, G., Eppenberger-Castori, S., Zlobec, I., Karamitopoulou, E., Arriga, R., Coppola, A., Caratelli, S., Spagnoli, G.C., Lauro, D., Lugli, A., et al. (2014). HLA Class II Antigen Expression in Colorectal Carcinoma Tumors as a Favorable Prognostic Marker. *Neoplasia* 16, 31–42. <https://doi.org/10.1593/neo.131568>.
36. Párrizas, M., Saltiel, A.R., and LeRoith, D. (1997). Insulin-like growth factor 1 inhibits apoptosis using the phosphatidylinositol 3'-kinase and mitogen-activated protein kinase pathways. *J. Biol. Chem.* 272, 154–161. <https://doi.org/10.1074/jbc.272.1.154>.
37. Kao, L.C., Germeyer, A., Tulac, S., Lobo, S., Yang, J.P., Taylor, R.N., Osteen, K., Lessey, B.A., and Giudice, L.C. (2003). Expression profiling of endometrium from women with endometriosis reveals candidate genes for disease-based implantation failure and infertility. *Endocrinology* 144, 2870–2881. <https://doi.org/10.1210/en.2003-0043>.
38. Burney, R.O., Talbi, S., Hamilton, A.E., Vo, K.C., Nyegaard, M., Nezhat, C.R., Lessey, B.A., and Giudice, L.C. (2007). Gene expression analysis of endometrium reveals progesterone resistance and candidate susceptibility genes in women with endometriosis. *Endocrinology* 148, 3814–3826. <https://doi.org/10.1210/en.2006-1692>.
39. Matsuzaki, S., Canis, M., Vaurs-Barrière, C., Boespflug-Tanguy, O., Das-tugue, B., and Mage, G. (2005). DNA microarray analysis of gene expression in eutopic endometrium from patients with deep endometriosis using laser capture microdissection. *Fertil. Steril.* 84, 1180–1190. <https://doi.org/10.1016/j.fertnstert.2005.04.041>.
40. Sherwin, J.R.A., Sharkey, A.M., Mihalyi, A., Sims, P., Catalano, R.D., and D'Hooghe, T.M. (2008). Global gene analysis of late secretory phase, eutopic endometrium does not provide the basis for a minimally invasive test of endometriosis. *Hum. Reprod.* 23, 1063–1068. <https://doi.org/10.1093/humrep/den078>.
41. Xu, Y., Lin, X., Xu, J., Jing, H., Qin, Y., and Li, Y. (2018). SULT1E1 inhibits cell proliferation and invasion by activating PPARgamma in breast cancer. *J. Cancer* 9, 1078–1087. <https://doi.org/10.7150/jca.23596>.
42. Cornel, K.M.C., Delvoux, B., Saya, T., Xanthoulea, S., Konings, G.F.J., Kruitwagen, R.P.F.M., Bongers, M.Y., Kooremann, L., and Romano, A. (2018). The sulfatase pathway as estrogen supply in endometrial cancer. *Steroids* 139, 45–52. <https://doi.org/10.1016/j.steroids.2018.09.002>.
43. Hirata, H., Hinoda, Y., Okayama, N., Suehiro, Y., Kawamoto, K., Kikuno, N., Rabban, J.T., Chen, L.M., and Dahiya, R. (2008). CYP1A1, SULT1A1, and SULT1E1 polymorphisms are risk factors for endometrial cancer susceptibility. *Cancer* 112, 1964–1973. <https://doi.org/10.1002/cncr.23392>.
44. Coan, M., Rampione Vinciguerra, G.L., Cesaratto, L., Gardenal, E., Bianchet, R., Dassi, E., Vecchione, A., Baldassarre, G., Spizzo, R., and Nicolo, M.S. (2018). Exploring the Role of Fallopian Ciliated Cells in the Pathogenesis of High-Grade Serous Ovarian Cancer. *Int. J. Mol. Sci.* 19, 2512. <https://doi.org/10.3390/ijms19092512>.
45. Cochrane, D.R., Tessier-Cloutier, B., Lawrence, K.M., Nazeran, T., Karnezis, A.N., Salamanca, C., Cheng, A.S., McAlpine, J.N., Hoang, L.N., Gilks, C.B., and Huntsman, D.G. (2017). Clear cell and endometrioid carcinomas: are their differences attributable to distinct cells of origin? *J. Pathol.* 243, 26–36. <https://doi.org/10.1002/path.4934>.
46. Low, S.E., and Nicol, A. (2004). Ciliated cell variant of endometrioid adenocarcinoma: a rare tumour. *J. Clin. Pathol.* 57, 1341–1342.
47. Dmowski, W.P., Ding, J., Shen, J., Rana, N., Fernandez, B.B., and Braun, D.P. (2001). Apoptosis in endometrial glandular and stromal cells in women with and without endometriosis. *Hum. Reprod.* 16, 1802–1808. <https://doi.org/10.1093/humrep/16.9.1802>.
48. Li, X.Y., Pi, Y.N., Chen, Y., Zhu, Q., and Xia, B.R. (2022). Nicotinamide N-Methyltransferase: A Promising Biomarker and Target for Human Cancer Therapy. *Front. Oncol.* 12, 894744. <https://doi.org/10.3389/fonc.2022.894744>.
49. Tseng, J.F., Ryan, I.P., Milam, T.D., Murai, J.T., Schriock, E.D., Landers, D.V., and Taylor, R.N. (1996). Interleukin-6 secretion in vitro is up-regulated ectopic and eutopic endometrial stromal cells from women with endometriosis. *J. Clin. Endocrinol. Metab.* 81, 1118–1122. <https://doi.org/10.1210/jc.81.3.1118>.

50. Steimle, V., Siegrist, C.A., Mottet, A., Lisowska-Grospierre, B., and Mach, B. (1994). Regulation of MHC class II expression by interferon-gamma mediated by the transactivator gene CIITA. *Science* 265, 106–109. <https://doi.org/10.1126/science.8016643>.
51. McLane, L.M., Abdel-Hakeem, M.S., and Wherry, E.J. (2019). CD8 T Cell Exhaustion During Chronic Viral Infection and Cancer. *Annu. Rev. Immunol.* 37, 457–495. <https://doi.org/10.1146/annurev-immunol-041015-055318>.
52. Shih, A.J., Adelson, R.P., Vashistha, H., Khalili, H., Nayyar, A., Puran, R., Herrera, R., Chatterjee, P.K., Lee, A.T., Truskinovsky, A.M., et al. (2022). Single-cell analysis of menstrual endometrial tissues defines phenotypes associated with endometriosis. *BMC Med.* 20, 315. <https://doi.org/10.1186/s12916-022-02500-3>.
53. Chen, S., Zhou, Y., Chen, Y., and Gu, J. (2018). fastp: an ultra-fast all-in-one FASTQ preprocessor. *Bioinformatics* 34, i884–i890. <https://doi.org/10.1093/bioinformatics/bty560>.
54. Dobin, A., Davis, C.A., Schlesinger, F., Drenkow, J., Zaleski, C., Jha, S., Batut, P., Chaisson, M., and Gingeras, T.R. (2013). STAR: ultrafast universal RNA-seq aligner. *Bioinformatics* 29, 15–21. <https://doi.org/10.1093/bioinformatics/bts635>.
55. Li, H., Handsaker, B., Wysoker, A., Fennell, T., Ruan, J., Homer, N., Marth, G., Abecasis, G., and Durbin, R.; 1000 Genome Project Data Processing Subgroup (2009). The Sequence Alignment/Map format and SAMtools. *Bioinformatics* 25, 2078–2079. <https://doi.org/10.1093/bioinformatics/btp352>.
56. Anders, S., Pyl, P.T., and Huber, W. (2015). HTSeq—a Python framework to work with high-throughput sequencing data. *Bioinformatics* 31, 166–169. <https://doi.org/10.1093/bioinformatics/btu638>.
57. Hao, Y., Hao, S., Andersen-Nissen, E., Mauck, W.M., Zheng, S., Butler, A., Lee, M.J., Wilk, A.J., Darby, C., Zager, M., et al. (2021). Integrated analysis of multimodal single-cell data. *Cell* 184, 3573–3587.e29. <https://doi.org/10.1016/j.cell.2021.04.048>.
58. Zhou, Y., Zhou, B., Pache, L., Chang, M., Khodabakhshi, A.H., Tanaseichuk, O., Benner, C., and Chanda, S.K. (2019). Metascape provides a biologist-oriented resource for the analysis of systems-level datasets. *Nat. Commun.* 10, 1523. <https://doi.org/10.1038/s41467-019-09234-6>.
59. Trapnell, C., Cacchiarelli, D., Grimsby, J., Pokharel, P., Li, S., Morse, M., Lennon, N.J., Livak, K.J., Mikkelsen, T.S., and Rinn, J.L. (2014). The dynamics and regulators of cell fate decisions are revealed by pseudotemporal ordering of single cells. *Nat. Biotechnol.* 32, 381–386. <https://doi.org/10.1038/nbt.2859>.
60. Efremova, M., Vento-Tormo, M., Teichmann, S.A., and Vento-Tormo, R. (2020). CellPhoneDB: inferring cell-cell communication from combined expression of multi-subunit ligand-receptor complexes. *Nat. Protoc.* 15, 1484–1506. <https://doi.org/10.1038/s41596-020-0292-x>.
61. Islam, S., Kjällquist, U., Moliner, A., Zajac, P., Fan, J.B., Lönnberg, P., and Linnarsson, S. (2011). Characterization of the single-cell transcriptional landscape by highly multiplex RNA-seq. *Genome Res.* 21, 1160–1167. <https://doi.org/10.1101/gr.110882.110>.
62. Li, L., Dong, J., Yan, L., Yong, J., Liu, X., Hu, Y., Fan, X., Wu, X., Guo, H., Wang, X., et al. (2017). Single-Cell RNA-Seq Analysis Maps Development of Human Germline Cells and Gonadal Niche Interactions. *Cell Stem Cell* 20, 858–873.e4. <https://doi.org/10.1016/j.stem.2017.03.007>.
63. Picelli, S., Faridani, O.R., Björklund, A.K., Winberg, G., Sagasser, S., and Sandberg, R. (2014). Full-length RNA-seq from single cells using Smart-seq2. *Nat. Protoc.* 9, 171–181. <https://doi.org/10.1038/nprot.2014.006>.

STAR★METHODS

KEY RESOURCES TABLE

REAGENT or RESOURCE	SOURCE	IDENTIFIER
Antibodies		
Mouse monoclonal anti-CD326	BioLegend	Cat#324208; RRID:AB_756081
Mouse monoclonal anti-CD10	Abcam	Cat#ab269339
Mouse monoclonal anti-CD45	BioLegend	Cat#368521; RRID:AB_2687375
Rabbit polyclonal anti-NNMT	Proteintech	Cat#15123-1-AP; RRID:AB_2153579
Rabbit monoclonal anti-FoxJ1	Abcam	Cat#ab235445; RRID:AB_10783267
Rabbit polyclonal anti-TPPP3	Abcam	Cat#ab150998; RRID:AB_2716739
Mouse multiclonal anti-pan Cytokeratin	Abcam	Cat#ab86734; RRID:AB_10674321
Rabbit monoclonal anti-CD4	MXB Biotechnologies	Cat#RMA-0620; RRID:AB_2925216
Mouse monoclonal anti-FOXP3	Abcam	Cat#ab20034; RRID:AB_445284
Rabbit monoclonal anti-HLA Class II DRB1	Abcam	Cat#ab133578
Mouse monoclonal anti-CD3	MXB Biotechnologies	Cat#MAB-0740
Mouse monoclonal anti-SULT1E1	Santa Cruz Biotechnology	Cat#sc-376009; RRID:AB_10990306
Rabbit monoclonal anti-alpha Tubulin (acetyl K40)	Abcam	Cat#ab179484; RRID:AB_2890906
AF647 donkey anti-rabbit	Abcam	Cat#ab150075; RRID:AB_2752244
AF488 donkey anti-mouse	Life Technologies	Cat#A21202; RRID:AB_141607
Rabbit monoclonal anti-FOXO1A	Abcam	Cat#ab52857
Rabbit polyclonal anti-Acetylated FOXO1	Thermo Scientific	Cat#PA5104560; RRID:AB_2816035
Rabbit monoclonal anti-BIM	Cell Signaling Technology	Cat#2933T
Rabbit monoclonal anti-GAPDH	Cell Signaling Technology	Cat#2118; RRID:AB_561053
Mouse anti-Human HLA-DR, DP, DQ	BD Bioscience	Cat#555556; RRID:AB_395938
Mouse monoclonal anti-CD28	Thermo Scientific	Cat#16-0289-81; RRID:AB_468926
Mouse anti-Human CD3	BD Bioscience	Cat#347344; RRID:AB_400286
Mouse anti-CD4	BD Bioscience	Cat#340672; RRID:AB_400532
Mouse monoclonal anti-CD8	BD Bioscience	Cat#562428; RRID:AB_11154035
Mouse monoclonal anti-IFN-γ	BioLegend	Cat#506506; RRID:AB_315440
Biological samples		
Normal endometrium from 11 healthy women	Peking University People's Hospital	N/A
Eutopic and ectopic endometrium from 23 patients with ovarian endometriosis	Peking University People's Hospital	N/A
Peripheral blood mononuclear cell	Peking University People's Hospital	N/A
Chemicals, peptides, and recombinant proteins		
DMEM/F-12 PLUS Basal Medium	Sigma	Cat#SCM162
Collagenase II	Thermo Fisher Scientific	Cat#17101015
Collagenase IV	Thermo Fisher Scientific	Cat#17104019
DNasel	Roche	Cat#11284932001
BSA	Thermo Fisher Scientific	Cat#15260037
7-AAD	BioLegend	Cat#420403
Zombie Fixable Viability Dye	Biolegend	Cat#423113
SuperScript™ II Reverse Transcriptase	Invitrogen	Cat#18064014
H ₂ O ₂	Sigma	Cat#7722-84-1
Goat serum	Sigma-Aldrich	Cat#S26-100ML
DAPI	Thermo Fisher Scientific	Cat#D1306

(Continued on next page)

Continued

REAGENT or RESOURCE	SOURCE	IDENTIFIER
Dynabeads MyOne Streptavidin C1 beads	Invitrogen	Cat#65605D
Lipofectamine™ RNAimax	Invitrogen	Cat#13778030
Magnetic beads	MilliporeSigma	Cat#130-050-101
RPMI 1640	Gibco	Cat#11875119
Human IL-2 Recombinant Protein	Gibco	Cat# 200-02-1MG
RIPA lysis	Thermo Scientific	Cat#89900
Protease inhibitor cocktail	Cell Signaling Technology	Cat#5871
PMSF	Thermo Scientific	Cat#36978
FBS	Thermo Scientific	Cat#A5256701
Penicillin-streptomycin	Sigma	Cat#P4333-20ML
IFN-γ	PeproTech	Cat#300-02-20UG
GolgiStop solution	BD Bioscience	Cat#51-2092KZ
Cytotix/Cytoperm™	BD Bioscience	Cat#554714
Critical commercial assays		
Kapa Hyper Prep Kit	Kapa Biosystems	Cat#KK8502
DAB Substrate Kit	MXB Biotechnologies	Cat#MAX007
Multiplexed IHC kit	Abcam	Cat#ab312827
<i>In Situ</i> Cell Death Detection Kit	Roche	Cat#11684795910
Deposited data		
scRNA-seq raw data	This paper	Genome Sequence Archive for Human: PRJCA009009
scRNA-seq data	Shih et al. ⁵²	Gene Expression Omnibus (GEO): GSE203191
Code	This paper	https://github.com/mengya98/endometriosis
Experimental models: Cell lines		
Immortalized Human Endometriotic Cell Line (12Z)	Applied Biological Materials Inc	Cat#T0764
Oligonucleotides		
See Table S6 for SiRNA sequences of NNMT	This paper	N/A
See Table S6 for SiRNA sequences of negative control	This paper	N/A
Software and algorithms		
fastp version 0.22.0	Chen et al. ⁵³	https://anaconda.org/bioconda/fastp
STAR version 2.6.0a	Dobin et al. ⁵⁴	https://github.com/alexdobin/STAR
samtools version 1.7	Li et al. ⁵⁵	https://anaconda.org/bioconda/samtools
HTSeq version 0.11.1	Anders et al. ⁵⁶	https://github.com/htseq/htseq
R Studio version 4.1.0	RStudio	https://cran.r-project.org/
Seurat version 4.1.0	Hao et al. ⁵⁷	https://www.satijalab.org/seurat
Metascape version 3.5	Zhou et al. ⁵⁸	https://metascape.org/gp/index.html
Monocle2 version 2.22.0	Trapnell et al. ⁵⁹	http://cole-trapnell-lab.github.io/monocle-release/docs/
CellphoneDB version 2.0	Efremova et al. ⁶⁰	https://github.com/ventolab/CellphoneDB
NDP.view2 U12388-01	Hamamatsu	https://www.hamamatsu.com/cn/zh-cn/product/life-science-and-medical-systems/digital-slide-scanner/U12388-01.html
CaseViewer version 2.4.0	3DHISTECH	https://www.3dhistech.com/solutions/caseviewer/
Flowjo v10	BD Biosciences	https://www.bdbiosciences.com/en-us/products/software/flowjo-v10-software
GraphPad Prism 9.0	Graphpad Prism Inc	https://www.graphpad.com/scientific-software/prism/
Other		
FACS Aria Sort	BD Biosciences	N/A
Covaris M220	Covaris	N/A
Illumina HiSeq 4000	Illumina	N/A

(Continued on next page)

Continued

REAGENT or RESOURCE	SOURCE	IDENTIFIER
Illumina NovaSeq 6000	Illumina	N/A
Nano Zoomer S360	Hamamatsu	N/A
Pannoramic SCAN II	3DHISTECH	N/A

RESOURCE AVAILABILITY**Lead contact**

Further information and requests for resources and reagents should be directed to and will be fulfilled by the lead contact, Fuchou Tang (tangfuchou@pku.edu.cn).

Materials availability

This study did not generate new reagents.

Data and code availability

- RNA-sequencing data have been deposited at Genome Sequence Archive for Human (PRJCA009009) and are publicly available as of the date of publication. Original western blot images, microscopy data and flow cytometry data reported in this paper will be shared by the [lead contact](#) upon request.
- Custom code developed in this study for differently expressed genes analysis, pseudotime analysis has been deposited at GitHub (<https://github.com/mengya98/endometriosis>) and is publicly available as of the date of publication.
- Any additional information required to reanalyze the data reported in this work paper is available from the [lead contact](#) upon request.

EXPERIMENTAL MODEL AND STUDY PARTICIPANT DETAILS**Human participants**

This study was approved by the Ethics Committee of Peking University People's Hospital (2020PHB154-01). All women with endometriosis and non-endometriosis controls included in the study underwent hysteroscopic surgery or laparoscopic surgery at the Peking University People's Hospital. To characterize the abnormalities of endometrium from patients, normal endometrium from 11 healthy women were used as controls; Eutopic and ectopic endometrium from 23 women with ovarian endometriosis were obtained (Table S1). Samples were obtained from women aged 26–48 years old with regular menstrual cycling (Table S1). Women with the following conditions were not enrolled in this study: recent contraception (intrauterine device usage in past 3 months; hormonal contraceptives in past 2 months), other uterine pathology (adenomyosis; bacterial, fungal or viral infection) or polycystic ovary syndrome.

Cell culture

Immortalized Human Endometriotic Cell Line (12Z, Applied Biological Materials Inc) were cultured in DMEM (Sigma) containing 10% FBS (ThermoFisher) at 37°C with 5% CO₂ in an incubator. T cells were isolated from peripheral blood mononuclear cells and were grown in suspended in RPMI-1640 Medium (Gibco) containing 10% FBS and 200 IU/mL IL-2 Recombinant Protein (Gibco) at 37°C with 5% CO₂ in an incubator.

METHOD DETAILS**Dissociation of tissue and flow cytometry**

Before dissociation, the tissue was rinsed with DMEM (Sigma, USA) on a Petri dish to remove blood and mucus. Excess DMEM was removed after rinsing. The tissue was then minced into pieces as small as possible and dissociated in 1.5 mg/mL collagenase II and collagenase IV (Thermo Fisher Scientific, USA) and agitated for 30 min at 37°C. 0.1 mg/mL DNase I (Roche, Switzerland) was added to the solution to digest extracellular genomic DNA. The digestion was quenched with DMEM. The cell suspension was then pipetted, filtered through a 70-μm cell strainer and centrifuged at 500 r.p.m. for 5 min. The pellet was resuspended with 0.5% BSA. CD326 antibody (BioLegend, USA), CD10 antibody (Abcam, UK) and CD45 antibody (BioLegend, USA) were incubated with single cells for 30 min at 4°C. 7-AAD (BioLegend, USA) was incubated for 5 min to exclude dead cells. Single cell was sorted by FACS Aria Sort (BD Biosciences, USA) into 96-well plate with lysis buffer.

Single-cell RNA-seq library construction

The single-cell RNA-seq library was produced using a modified STRT-seq methodology.^{61–63} After the cells were lysed to release all of their RNA, an oligo-dT primer containing an anchor sequence, a cell barcode, and a unique molecular identification (UMI) sequence

was used to capture the mRNAs. Reverse transcription enzyme (Invitrogen, USA) was used to transcribe the mRNAs into first-strand cDNAs. Pre-amplification (18 cycles) was the next step to boost cDNA yields. In the end, cDNAs from individual cells were barcoded, and cDNAs from different cells were combined with different barcodes. The index sequence with a biotin modification was added to the 3' ends of the cDNAs following 4 cycles of PCR. Then Covaris M220 sheared DNA into 300bp fragments and enriched by Dynabeads MyOne Streptavidin C1 beads (Invitrogen, USA). Finally, we used Kapa Hyper Prep Kit (Kapa Biosystems, USA) to construct library and sequenced with Illumina HiSeq 4000 and NovaSeq 6000.

Analysis of single cell RNA-Seq data

After the data was downloaded, we removed the adaptor sequence and use fastp version 0.22.0 to make quality control.⁵³ In this paper, the proportion of reads that pass the quality control of the raw data is more than 80%. Quality-controlled reads were aligned to the human genome reference hg38 using the STAR version 2.6.0a.⁵⁴ After that, we used samtools version 1.7 to index and remove duplicates of the aligned bam, HTSeq version 0.11.1 was used for gene quantification ("htseq-count -s no -f bam -a 10").^{55,56} Finally, we used UMI (unique molecular identifier) to remove the gene expression number error introduced in the PCR process. Through the processing above, we got the gene expression matrix. To retain the high-quality single-cell data, total genes count and mitochondrial genes count were used as the standard to filter low-quality cells. Cells with reads counts less than 10000 or more than 1500000 were filtered out. So did the cells with mitochondrial reads counts account for more than 25% of the total reads counts. After these elementary quality control, 7030 cells were retained for downstream analysis. Gene expression levels were transformed into ln(TPM+1). To classify cell types, we utilized the Seurat R package version 4.1.0 to obtain 3500 highly variable genes, which were used to perform principal component analysis (PCA).⁵⁷ The clustering parameter resolution was set to 0.4 for the function FindClusters in Seurat. We used UMAP (Uniform Manifold Approximation and Projection) for visualization of clusters. We identified differentially expressed genes using Wilcoxon Rank-Sum test among different cell types with the function FindAllMarkers and FindMarkers in the Seurat package. DEGs based on the following criteria were selected: (1) Avg_log₂(Fold Change) > 0.25; (2) Adjusted p value ≤ 0.05. GO analyses were performed using Metascape version 3.5, and significantly enriched biological process GO terms were selected.⁵⁸ Monocle2 version 2.22.0 was applied to perform pseudotime analysis and decipher the transcriptional trajectories of epithelial cells based on 1000 highly variable genes.⁵⁹

Cell interaction analysis

To explore the potential interactions among different cell types in the endometriosis lesions, we performed ligand-receptor interaction analysis using CellphoneDB version 2.0.⁶⁰ CellphoneDB integrated multiple protein-protein interaction databases, to figure out the potential interactions. The data was preprocessed using Seurat, in which the raw data of the Seurat object was normalized to total reads 1000000 each cell. And the cell types were classified by Seurat, consistent with the former descriptions. The analysis was performed using the default parameters and only the interactions with the p value less than 0.05 and the expressions of both the ligand and receptor were greater than 0 were retained.

IFN-γ signature scoring

We applied the function AddModuleScore in Seurat R package to detect the IFN-γ signature. The function AddModuleScore could calculate the average expression levels of each program (cluster) on single cell level, subtracted by the aggregated expression of control feature sets. All analyzed features are binned based on averaged expression, and the control features are randomly selected from each bin.

Immunohistochemistry

For immunohistochemistry, 5-μm-thick formalin-fixed paraffin-embedded (FFPE) tissue sections were deparaffinized in xylene, and rehydrated through graded ethanol solutions after being baked at 65°C for 2 h. Following heat-mediated, sodium citrate antigen retrieval (pH6), slides were treated with 3% H₂O₂ to quench endogenous peroxidase activity, washed, incubated with 5% goat serum to block nonspecific binding sites, and stained with primary antibodies (NNMT antibody (1:1000), Proteintech, USA; FOXJ1 antibody (1:500), Abcam, UK; TPPP3 antibody (1:200), Abcam, UK) overnight at 4°C. After primary antibody staining, slides were processed with the polymeric horseradish peroxidase (HRP)-conjugated secondary antibody (Abcam, UK) and DAB Substrate Kit (MXB Biotechnologies, CHN). Slides were counterstained with hematoxylin and dehydrated through graded alcohols and xylene. Sections were scanned by slide scanners (Nano Zoomer S360) and viewed with NDP.view software (NDP.view2 U12388-01, Hamamatsu).

Immunofluorescence staining of FFPE tissue

For multiplex immunofluorescence staining of FFPE tissue, slides were performed using Bioss Multiplexed IHC kit according to manufacturer's instruction. The slides were microwave heat-treated after each tyramide signal amplification operation. Pan-cytokeratin (ab86734, Abcam, UK), CD4 (RMA-0620, MXB Biotechnologies), FOXP3 (ab20034, Abcam), HLA-DRB1 (ab133578, Abcam), CD3 (MAB-0740, MXB Biotechnologies), FOXJ1 (ab235445, Abcam), TPPP3 (ab150998, Abcam), SULT1E1 (sc-376009, Santa Cruz Biotechnology), acetylated α-tubulin (ab179484, Abcam) antibodies were applied for different panel in the figures. Primary antibodies in a panel from different host species were incubated with AF647 donkey anti-rabbit antibody (ab150075, Abcam) and AF488 donkey anti-mouse antibody (A21202, Life Technologies). Primary antibodies in a multiplexed panel from the same host species were

incubated with horseradish peroxidase-conjugated secondary antibody and tyramide signal amplification. Nuclei were stained with DAPI after all the antigens above had been labeled. The stained slides were scanned to obtain multispectral images using the Panoramic SCAN II (3DHISTECH, Budapest, Hungary) and viewed with CaseViewer software (3DHISTECH, version 2.4.0). The distance between cells was measured using tool that come with the CaseViewer software. Receiver operating characteristic (ROC) curve analysis was performed to evaluate HLA-DRB1 levels. Indicated by the maximum value of the Youden index, HLA-DRB1 expression levels was classified as “high” and “low”.

NNMT knockdown by siRNA

The siRNA targeting NNMT and control siRNA were designed and synthesized by Tsingke Biotechnology Co., Ltd. (Beijing, China). Briefly, 12Z cells were seeded on six-well plates to reach 60–70% confluence and transfected with 60 nM siRNA targeting NNMT or the control siNC using Lipofectamine RNAiMAX (Invitrogen, USA) transfection agent according to the manufacturer’s instructions. Incubated for 48 h at 37°C, cells are used for immunofluorescence staining for FOXO1A, acetylated FOXO1 and BIM or immunoblot experiments.

Immunoblots

Cells were lysed in SDS lysis buffer containing RIPA lysis (89900, Thermo Scientific), protease inhibitor cocktail (5871, Cell Signaling Technology) and PMSF (36978, Thermo Scientific). Collected cell pellets were lysed with lysis for 5 min and centrifuged at 14000 r.p.m for 15 min at 4°C. The supernatant is collected for immunoblotting. Capillary-based immunoassay was performed using the Wes-Simple Western method for detection of NNMT (15123-1-AP, Proteintech), FOXO1 (ab52857, Abcam) and acetylated FOXO1 (PA5104560, Thermo Scientific). GAPDH (2118, Cell Signaling Technology) was used as loading control. Jess-Simple Western method was used for BIM (2933T, Cell Signaling Technology) detection. Protein expression was measured by chemiluminescence and quantified as area under the curve using the Compass for Simple Western program (ProteinSimple).

TUNEL staining

Apoptotic cells were detected by *In Situ* Cell Death Detection Kit (11684795910, Roche). Adherent cells were fixed with 4% PFA for 20 min and permeabilized with 0.1% Triton X-100 for 5 min at room temperature. Cells were then incubated with 50 µL TUNEL reaction mixture at 37°C for 1 h. Nuclei was stained with Hoechst 33342 (H3570, Invitrogen).

Co-culture assay

12Z cells, an SV40-transformed endometriotic epithelial-like cell line derived from peritoneal endometriosis lesions, was maintained in DMEM/F12 supplemented with 10% FBS and 1% penicillin-streptomycin in a humidified atmosphere of 5% CO₂ at 37°C. Human peripheral blood mononuclear cells (PBMC) from healthy donors were isolated by Ficoll-Hypaque density-gradient centrifugation. CD3⁺ T cells were isolated from PBMC using magnetic beads (Miltenyi Biotec, Germany) according to the manufacturer’s protocol and then suspended in RPMI-1640 Medium containing 10% FBS. 12Z cells were stimulated with 200 ng/mL human IFN-γ (PeproTech, USA) for 48h to express HLA class II. HLA class II block group was incubated with HLA class II antibody (5 µg/ml, BD, USA) for 30 min at 4°C. HLA class II⁺ and HLA class II⁻ blocked 12Z cells were respectively seeded on 48-well plates precoated with anti-CD28 antibodies at a density of 3 × 10³ cells per well, then CD3⁺ T cells were added and co-cultured with HLA class II⁺ and HLA class II blocked 12Z cells at a 10:1 ratio (T cells: Epithelial cells) for 12 h. GolgiStop solution (BD, USA) were added to prevent secretion of cytokines.

Flow cytometry

After co-culture, T cells were collected and first incubated with Zombie Fixable Viability Dye (Biolegend, USA) at room temperature for 15 min. Then they were incubated with the following surface antibodies: CD3-PerCP (347344, BD Bioscience), CD4-APC (340672, BD Bioscience) and CD8-BV421 (562428, BD Bioscience) at 4°C for another 30 min. After fixed and permeabilized using BD Cytofix/CytopermTM (BD, USA), they were stained with IFN-γ-PE antibody (506506, BioLegend) at 4°C for 30 min. The cells were finally washed twice and resuspended in PBS. FACSCanto II (BD Biosciences) and Flowjo software were used to analyze the percentage of IFN-γ⁺ T cells.

QUANTIFICATION AND STATISTICAL ANALYSIS

Data analysis of sequencing data

Single cell RNA-seq was performed on 23 patients with ovarian endometriosis and 11 healthy women with STRT-seq method as described in the [method details](#). Differentially expressed genes (DEG) were identified by Wilcoxon Rank-Sum test using function FindAllMarkers and FindMarkers in the Seurat package, which was also described in the [method details](#). GO analyses were performed by Metascape3, and some of significantly enriched biological process GO terms that corresponding p values were less than 0.01 were selected.

Experimental data analysis

The statistical diagrams and statistical tests were conducted in GraphPad Prism9. The statistical test and numbers used for each comparison is denoted in the corresponding figure legend. The statistical test for percentage of FOXJ1⁺ cells in eutopic and ectopic endometrium, and activated T cells in co-culture assays was paired *t* test. The statistical test for NNMT and TUNEL positive cells was Mann-Whitney test. Other statistical test for experimental data was Two-tailed *t* test. The statistical test for single-cell data analysis was Wilcoxon rank-sum test. The correspondence between symbols and significance values: *, p ≤ 0.05; **, p ≤ 0.01, ***, p ≤ 0.001; ****, p ≤ 0.0001. The bar graphs were shown by mean with SEM.